On the turbulence modeling and conjugate heat transfer study of the cooling system of the Beam Dump Facility target at CERN

Steady and Transient Analysis

Mayank Pandey

Technische Universiteit Delft

TU Delft Delft University of Technology

Challenge the future

On the turbulence modeling and conjugate heat transfer study of the cooling system of the Beam Dump Facility target at CERN

Steady and Transient analysis

by

Mayank Pandey

in partial fulfillment of the requirements for the degree of

Master of Science
in Mechanical Engineering

at the Delft University of Technology,
to be defended publicly on Wednesday December 19, 2018 at 14:30 PM.

Student number:	4618653	
Thesis committee:	Prof. dr. ir. B. J. Boersma,	TU Delft, Supervisor
	Dr. H. Nemati,	TU Delft, Supervisor
	Ir. E. Lopez Sola,	CERN, Supervisor
	Dr. Ir. M. Calviani,	CERN, Supervisor
	Dr. Ir. M. Pourquie,	TU Delft
	Dr. Ir. J. Peeters,	TU Delft

This thesis is confidential and cannot be made public until December 19, 2018.

TU Delft Delft University of Technology

TU Delft Delft University of Technology CERN

Acknowledgement

This thesis was not possible in it's present form without the continuous support and guidance of my supervisors at CERN, Ir. E. L. Sola and Dr. Marco Calviani and my supervisors at TU Delft Prof. dr. ir. B.J. Boersma and Dr. ir. Hassan Nemati. I would like to thank Marco specifically for providing me the opportunity to work at the excellent facility of TCD section at CERN. I pay my gratitude to the members of my thesis committee Dr. ir. M. Pourquie and Dr. ir. J. Peeters for taking out their precious time to evaluate my performance. The continuous discussions with Ir. Pietro Avigni, Ir. Rui Franqueira and Ir. Maqsood Alam from CERN is highly appreciated. I would also like to thank my friends (Navdeep, Jayant, Nikolay, Athina, Paul etc.) and well-wishers for supporting me in tough times during this journey of my MSc degree programme. Finally, I am grateful to my family who provided this excellent opportunity to me for pursuing my dreams at one of the finest university. I thank them for their financial and emotional support.

Mayank Pandey
Delft, December 2018

Abstract

The Beam Dump Facility (BDF) is a new fixed target facility proposed to be installed in the North Area of CERN. Currently in its design phase, the BDF is aimed at the Search for Hidden Particles (SHiP) experiment, which purpose is to investigate the origin of dark matter and other lightly interacting particles. The BDF target/dump sits at the core of the installation, and its aim is to fully absorb the high intensity Super Proton Synchrotron (SPS) beam and produce charmed mesons. The average beam power on target is 305 kW due to which very high thermo-mechanical loads will be generated on the target/dump configuration which can lead to mechanical failure of the target material. This calls for continuous cooling and heat removal from the target material, which requires the design and optimization of a very complex cooling system to ensure the target reliability during operation.

Keeping in view the high velocities that are obtained in the channels of the cooling system of the target assembly, an extensive 3D turbulence modeling of the full scale cooling system is required in order to predict the target water cooling system behavior. A comparative conjugate heat transfer (CHT) study using a simplified 2D geometry of the BDF target for different mesh size was performed for identical y^+ values to validate the pressure drop in the cooling channels and the temperature profile in the target blocks with the analytical calculations. Subsequently, a 3D model of the cooling channel was simulated for different Reynolds number and an extensive study was performed to check the behaviour of the flow in the log-law layer. In addition to that the friction factor was validated with the analytical results and with the available literature for various Reynolds number. Thereafter a full scale 3D steady and transient model was simulated using the information obtained from the previous studies. All these simulations were carried out in Ansys Fluent. The energy deposition in space on the target blocks was obtained via FLUKA MonteCarlo simulations. The variation of HTC in different channels and the fluid-solid interface temperature is found out to be in accordance with the analytical calculations. The pressure drop and the temperature rise from inlet to outlet of the cooling system is also in confirmation with the design parameters. Transient simulations were performed subsequently in order to study the impact of time and space varying energy deposition in the target blocks on the overall flow. With the given inlet velocity, the boiling at the surface of the target blocks is not expected to happen. As a final part of this study, in order to make the numerical model more robust, a mesh sensitivity analysis was done in order to optimize the mesh size, especially in the boundary layer region.

Nomenclature

ΔP	Pressure drop
$\dot{m}$	Mass flow rate
ϵ	Rate of dissipation of turbulence energy
μ	Dynamic viscosity
ω	Specific rate of dissipation of k
$\overline{u}$	Average fluid velocity
ρ	Density
c	channel
D_H	Hydraulic diameter
f	friction factor
i	inlet
k	Thermal conductivity
Nu	Nusselt number
Pr	Prandtl number
Re_D	Reynolds number
T_{ref}	Reference temperature
T_{sat}	Saturation temperature of water
u^+	Non-dimensional mean velocity
v_c	Channel velocity
y^+	Non-dimensional wall distance
GeV	Giga electronvolt
h	Heat Transfer Coefficient
k	Turbulent kinetic energy
Q	Power deposited on the target
SST	Shear stress transport
TeV	Tera electronvolt
TZM	Titanium Zirconium Molybdenum
W	Tungsten

Contents

List of Figures

List of Tables

1

Introduction

The European Organization for Nuclear Research (CERN) is the world's largest particle physics laboratory which is located near Geneva at the Swiss-French border. Founded in 1952, the physicists and engineers at CERN are investigating the fundamental structure of the universe by using world's largest and most complex scientific instruments. In its several experimental facilities, the particle beams (close to the speed of light) are made to collide together or with a fixed target, with the idea of studying the very basic constituents of matter in order to complete the Standard Model. These experiments provide insights to the physicists about the fundamental laws of nature by studying the phenomenon of particle interaction[1].

1.1. CERN Accelerators

Within the framework of CERN's experiment, the particle interactions usually takes place by bombarding charged protons or ions with other particles circulating in opposite direction or with a target and thereby producing a shower of particles. The primary aim of these experiments is to reproduce the phenomenon like Big Bang which occurred around 13.8 billion years ago and thereby giving the scientists an opportunity to study new particles in order to explain the creation of Universe. The particle interaction which usually takes place at high energy and close to the speed of light is facilitated by CERN accelerators. The particles are steered and accelerated in these machines using electromagnetic fields. A schematic diagram of the CERN's accelerator complex is shown in figure 1.1.

[1] http://home.cern/about

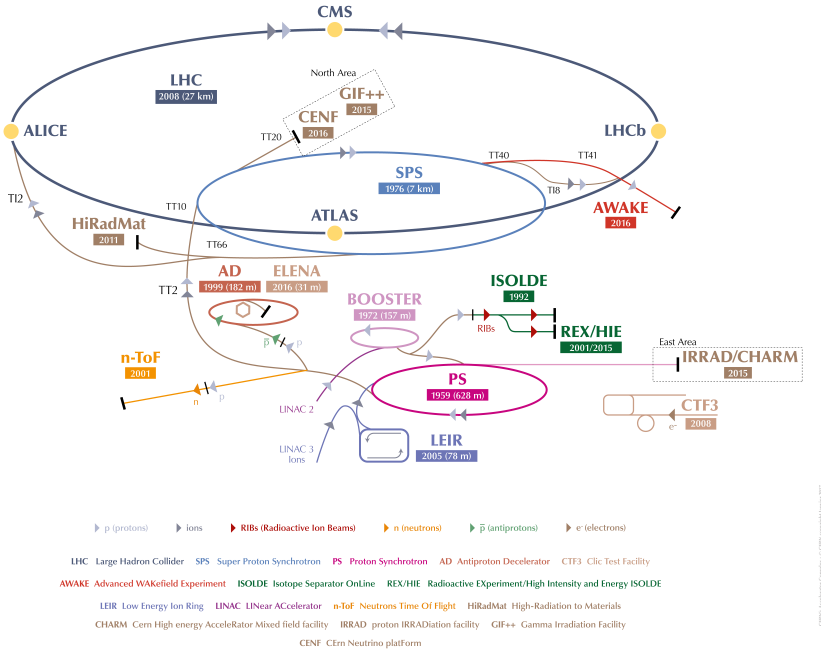

Figure 1.1: ***CERN Accelerator Complex***

The particle beam for Large Hadron Collider (LHC), is produced by the Hydrogen atoms from a compressed gas cylinder which is feeded at a controlled rate to the linear accelerator known as LINAC-2. The protons from these Hydrogen atoms are accelerated until the one-third of the speed of light and they achieve 50 MeV of energy (the energy of a particle is measured in electronvolt or eV). These packet of protons then enter the Proton Synchroton Booster (PS Booster) which is circular in shape with 157 metres circumference. This is done to accelerate the proton packets until 91.6% of the speed of light and to increase it's energy to 1.4 GeV. It is then feeded to the Proton Synchroton (PS) which is 628 meters in circumference and here the proton packets attains 99.93% of the speed of light and an energy of 26 GeV. Subsequently, the proton packets are channeled into the Super Proton Synchroton (SPS) which is 7 km in circumference. At this stage, the energy of protons is increased to 400 GeV. The proton beam to the LHC, is supplied from the SPS stage into two counter-rotating beams, each reaching very close to the speed of light and upto the energy of 7 TeV (7000 times heavier than at rest). The LHC is 26.7 km in circumference and facilitates four collision points in the tunnel where the debris from the collisions of counter-rotating beams are detected. The energy as high as 14 TeV is reached at these collision points which becomes possible because of the superconducting magnets installed in the LHC tunnel where the temperature is even lower than that in the outer space. The four experimental locations at these collision points are A Toroidal LHC Apparatus (ATLAS), Compact Muon Solenoid (CMS), A Large Ion Collider Experiment (ALICE) and LHC-beauty (LHCb). Every experimental site has it's own unique detectors which are used to collect and study the data obtained after the collision. It provides physicists from all over the world an opportunity to study these collisions and to discover particles like Higgs-Boson, which was discovered from these collisions by the collected effort of ATLAS and CMS in 2012.

CERN's accelerators are also used to accelerate other particles like Lead ions which are channeled to The Low Energy Ion Ring (LEIR) [9] through LINAC3 and subsequently fed to the LHC ring via a similar procedure as described above. In addition to the main experimental sites (ATLAS, CMS ALICE and LHCb) in the LHC ring, there are several other experiments of high importance which get beam directly from the accelerators complex. For instance, the Antiproton Decelerator (AD) and the Neutron Time of Flight (n-ToF) facilities receive proton

beam directly from the PS and the High Radiation to Materials (HiRadMat) facility gets the proton beam from SPS. In the similar line of experimental facilities, the proposed Beam Dump Facility (BDF) will also receive proton beam from the SPS accelerator.

1.2. Beam Intercepting Devices

The Targets, Collimators and Dumps (TCD) section of the Sources, Targets and Interactions (STI) group which comes under the Engineering (EN) department of CERN is responsible for all the Beam Intercepting Devices (BID) installed in the accelerator complex of CERN. The section is responsible for the conceptual studies, manufacturing, installation and maintenance of the mechanical systems and equipment associated to all the beam intercepting devices. In addition to that, the TCD section, in collaboration with the Fluka Development and Applications (FDA) section, is also responsible for the development of high-energy targets and dumps based on the FLUKA [39] study results [2]. BID are all those devices which interact with the particle beam for explicit purposes and can be broadly categorized into 3 main groups:

- **TARGETS**: A target is a device which emits a shower of secondary (charged and neutral) particles when a beam of accelerated particles impacts to it. It can be made up of solid, liquid or gas material.
- **DUMPS**: A dump is a device usually made up of low density material, whose objective is to safely absorb the particle beam when not required anymore. They are used in all the accelerators and acts as a safety valve for the experiments.
- **COLLIMATORS**: A collimator is a device which is used for narrowing down a particle beam. This process is also known as ”cleaning of beam” which means that beam will minimally spread in transverse direction as it propagates. A collimator is used in the accelerators in order to protect the instrumentation which are installed in the vicinity of the beam propagation tunnel.

1.3. Beam Dump Facility

The proposed BDF facility [13] will use the 400 GeV/c proton beam from the SPS accelerator. The Search for Hidden Particles (SHiP) experiment [34] will be the first experiment to utilize this facility whose aim is to explore the dark matter by the study of weakly interacting particles like charmed mesons. The beam characteristics used for this experiment is given in table 1.1.

Table 1.1: ***Beam parameters***

Proton momentum [GeV/c]	400
Beam intensity [p+/cycle]	$4.0 \cdot 10^{13}$
Cycle Length [s]	7.2
Spill duration [s]	1.0
Average beam power on target [kW]	305
Average beam power on target during spill [MW]	2.2

In the above table, the beam intensity signifies the number of protons impacting the target in one cycle. During one cycle of $7.2s$, the actual beam impact time with target is $1s$ which is also known as spill or pulse duration. Figure 1.2 illustrates the cycle and the pulse duration. The aim of the experiment is to deposit $4 \cdot 10^{19}$ protons on target (POT) per year.

[2] http://en.web.cern.ch/en-sti-group

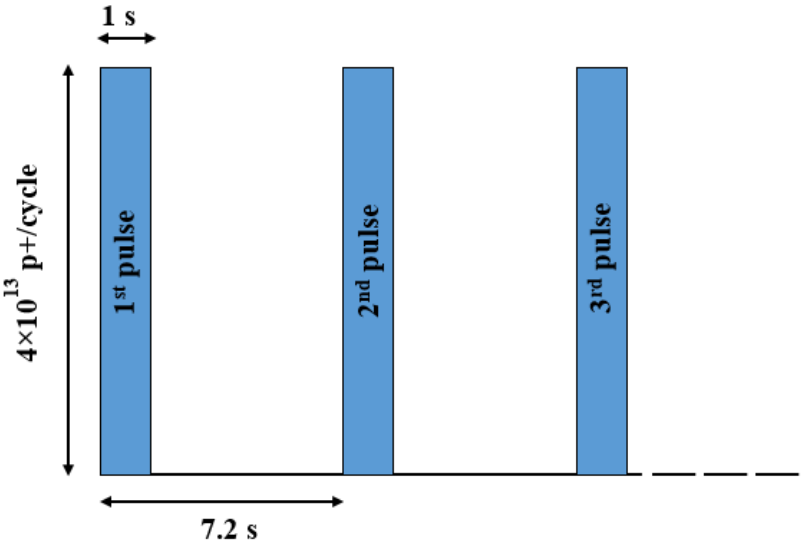

Figure 1.2: ***Cycle and pulse duration along with proton per pulse***

1.3.1. BDF Target Design

The BDF target is made of 18 concentric circular cylinders having a diameter of 250mm. Each block is maintained at a distance of 5mm from each other thereby forming several channels for the flow of water through it, which is used as a coolant in BDF cooling system. Because of the high energy deposition on target, the design and optimization of an effective cooling system is one of the most important aspects of this project. The high speed water flow through the cooling channels between consecutive target blocks will dissipate the power deposited by the proton beam. The total effective length of the target with and without considering the cooling channels is 1.36m and 1.455m respectively. Figure 1.3 shows a schematic of the BDF target core with first 13 blocks made of an alloy of Titanium, Zirconium and Molybdenum (TZM) and the remaining 5 blocks made up of Tungsten (W). All the blocks are cladded with Ta2.5W (represented by light turquoise color), which is a Tantalum alloy with 2.5% content of Tungsten.

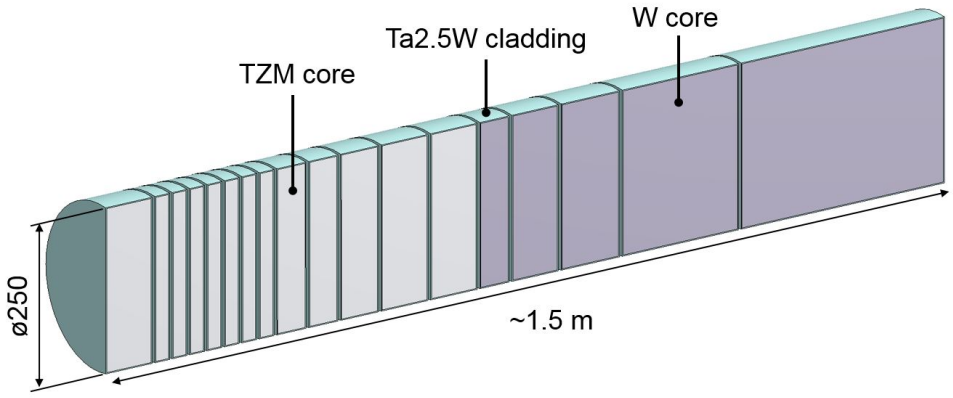

Figure 1.3: ***Schematic of Beam Dump Facility target core***

Table 1.2: ***BDF target length and materials***

Target number	Target material	Cladding material	Length [mm]
1	TZM	Ta2.5W	80
2	TZM	Ta2.5W	25
3	TZM	Ta2.5W	25
4	TZM	Ta2.5W	25
5	TZM	Ta2.5W	25
6	TZM	Ta2.5W	25
7	TZM	Ta2.5W	25
8	TZM	Ta2.5W	25
9	TZM	Ta2.5W	50
10	TZM	Ta2.5W	50
11	TZM	Ta2.5W	65
12	TZM	Ta2.5W	80
13	TZM	Ta2.5W	80
14	W	Ta2.5W	50
15	W	Ta2.5W	80
16	W	Ta2.5W	100
17	W	Ta2.5W	200
18	W	Ta2.5W	350

Ideally, the production of weakly interacting particles like charmed mesons will be maximized, if a single cylindrical target of length $1.36m$ is used. However, in such a case the thermal stresses being developed in the target due to large power deposition will lead to the mechanical failure of the target material. Hence it was imperative to optimize the $1.36m$ long target into several parts so that each part reaches a uniform energy deposition. The target material and the optimized length of each target is shown in table 1.2. The total power deposition and energy deposition per unit volume in each block is illustrated in figure 1.4 and 1.5 respectively.

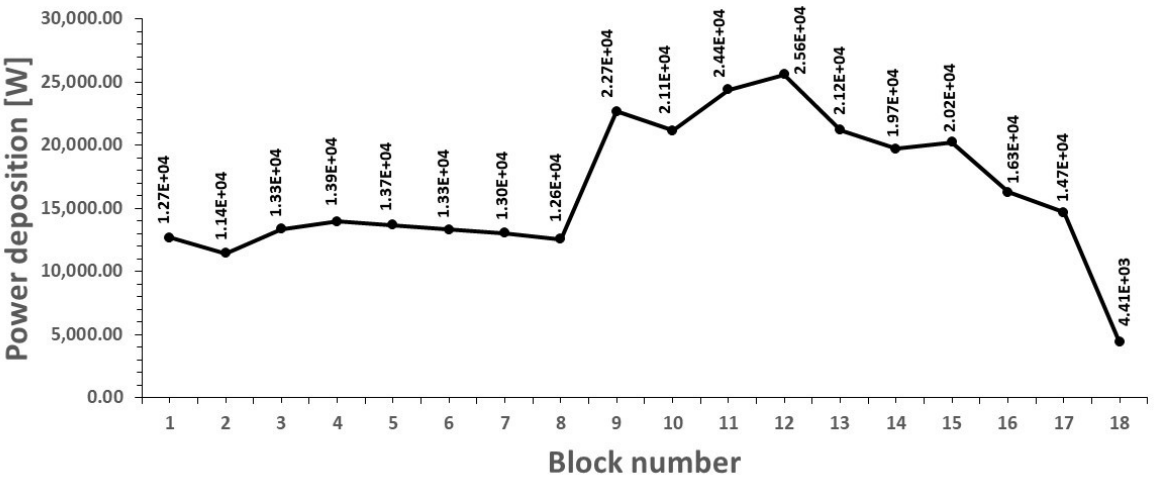

Figure 1.4: ***Total power deposition in each block of the BDF target***

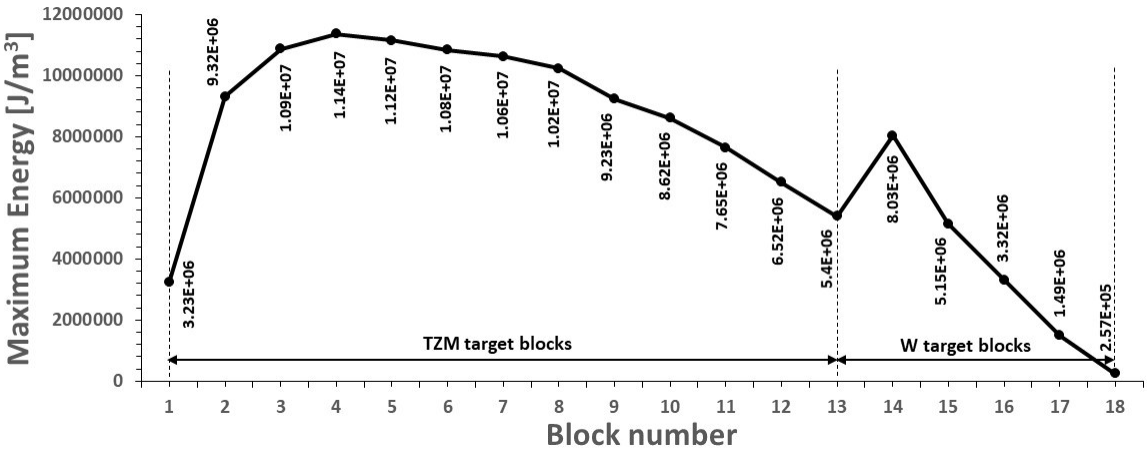

Figure 1.5: ***Maximum energy deposition per unit volume in the BDF target***

During the time period when proton beam impacts with the target, most of the beam energy is deposited in the first 13 blocks (as illustrated in figure 1.5). For this reason TZM (Titanium, Zirconium and Molybdenum alloy) was used as the material for these target blocks which has high strength and re-crystallization temperature. For the remaining 5 blocks which receives comparatively less energy, Tungsten (W) was used. The choice of Tungsten as the material was primarily based on the requirement of the experiment from physics point of view (high atomic number and short interaction length) and its good performance under irradiation. All the target blocks are cladded with a $1.5mm$ coating of Ta2.5W, to prevent the target blocks from getting corroded/eroded due to high speed water streams flowing in the cooling channels during operation. The mechanical properties of TZM, W and Ta2.5W at room temperature are given in table 1.3, however temperature dependent properties for the target material were used in the numerical simulations, which is given in appendix A.

Table 1.3: ***Mechanical properties of TZM, W and Ta2.5W at room temperature***

Properties	TZM	W	Ta2.5W
Density, ρ $[kg/m^3]$	10200	19250	16663
Specific Heat, C_p $[kJ/kg.K]$	267	132	140.68
Thermal Conductivity, k $[W/m.K]$	118	173	55.38

With such high beam power on target, the continuous and concentrated impact of it at one location would mean mechanical failure. Keeping this in mind, the beam is diluted by the upstream magnets following a circular pattern having a radius of $50mm$, beam size of $8mm$ (1σ) and with 4 equal turns in the pulse duration. This facilitates similar beam interactions on target with less mechanical stress. Figure 1.6 shows a representational diagram of beam impact with the target however a more comprehensive illustration of energy and temperature distribution on the blocks is given in section 4.2 where it will be shown that the energy distribution due to the proton beam on the target blocks is non-uniform in nature. In the given figure, the beam is represented by red color with a thickness of $16mm$ and the grey colored circular cylinders represent target blocks. In figure 1.6, part a.) shows the 3D view of the beam impact with the target and part b.) shows the left sided 2D view.

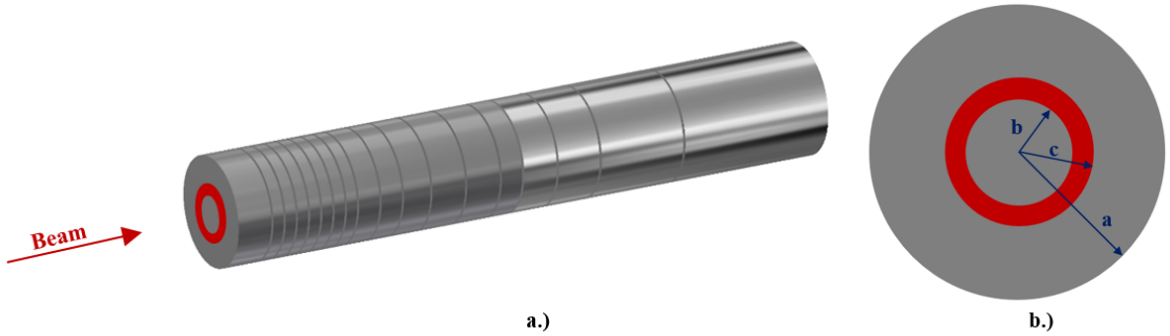

Figure 1.6: ***A representational figure to show the beam impact with the target where a = 125mm, b = 42mm and c = 58mm.***

1.4. Literature review

The design and optimization of the BDF target's cooling system is one of the most challenging aspect of the project due to the high energy and power deposition reached during the beam impact as shown in figures 1.5 and 1.4. The conceptual design of the BDF target's cooling system (with water as the coolant) is ongoing since many years [22]. In its early phase, contrary to the present design, there were 17 target blocks and all of them had similar cross-section ($0.3 \times 0.3 m^2$). A volumetric flow rate of $180 m^3/h$ with an operational pressure of 10 bar was used for the CFD simulations [29]. Higher volumetric flow rate was necessary for this design to achieve the desired cooling because of the absence of blockers (or dividers). The analysis of the cooling system based on this study recommended to use higher operational pressure or mass flow rates to avoid boiling at the target water interface and to achieve desired stresses in the target blocks.

Similar studies on the cooling system of the other spallation target sources ([27], [11], [41], [4]) with different power deposition on the target has been performed by researchers and engineers around the world. For the cooling system of the TRADE spallation target [43], water at a flow rate of $8 m^3/h$ was selected to cool the solid Tantalum target bombarded by the proton beam. It was reported that the results using different turbulence models ($k-\omega$ SST, $k-\epsilon$ RNG etc.) gave results which were in good agreement between different CFD codes used by different institutions involved in the project. The boiling scenario, which leads to the inhibition of heat transfer to the fluid was also avoided. Dan Wilcox [41] performed the design and optimization of the ISIS TS1, where Tantalum cladded Tungsten was used as the target which employs $800 MeV$ energy proton beam. Several designs for the cooling manifold were considered with an aim to minimize the pressure drop and the water volumetric flow rate and to minimize overheating if one channel becomes partially blocked. Straight manifold with no divider was reported to give the optimum flow distribution. The thermal-hydraulic study of Sodium-cooled Tungsten target for a $5 MW$ (600 MeV) proton beam was performed by Cheng et al. [42]. Two configurations (horizontal and vertical) of the Tungsten plates were considered with the Sodium flow velocity of $5 m/s$ in the cooling channels. It was reported that under normal conditions, the cladding and the tungsten plates were sufficiently cooled for a cladding thickness of $0.5 mm$ or less.

Kraus et. al [4] performed the detailed CFD analysis of the Tungsten and Uranium target geometry which was bombarded by an electron beam ($100 kW$, $100 MeV$) and where water was used as the coolant. Realizable $k-\epsilon$ and $k-\omega$ SST turbulence models were used to analyze the flow behaviour in the cooling system. Flow instabilities were reported in the manifold which didn't had significant temperature fluctuations in the target and the boiling point was not reached in the water-target interface which was favourable for the overall heat transfer. The cooling characteristics of the ISIS Tantalum target was studied experimentally by Allen et al. [15] at the Rutherford Appleton Laboratory in UK where heavy-water was used as the coolant. The cooling system in this case employs three different loops with an aim to supply the similar high velocity flow rate for each of the inter-plate coolant channels. The

cooling of the target plates was found to be in accordance with the Newton's law of cooling. A considerable reduction in cooling efficiency was reported after an irradiation of nearly $1Ah$ with 800 MeV protons. Jollet et al. [36] performed the numerical flow simulation of the Swiss spallation source, SINQ. This spallation uses the Cannelloni rod bundle as the target material which is bombarded by the proton beam and cooled by the heavy water (D_2O). The pressure based coupled algorithm with second-order formulation was used to solve the flow and heat transfer problem. $k-\omega$ SST turbulence model of Fluent [1] was used in this study because of it's robustness to resolve the flow behaviour near the wall and the far-field region. The heat transfer coefficients obtained from this study was given as an input to the FEM simulations for the stress analysis. The design and the development of the CSNS target system was performed by Quan Ji et al. [14] which employs Tungsten target cladded by Tantalum which is bombarded by a proton beam ($1.6GeV$ and $200kW$) and cooled by the heavy water (D_2O). The cross section of the target used in this study is $50 \times 130\ mm^2$ and the length is $607.5mm$. The target is divided into 15 plates and two different cooling assemblies are used with different flow velocities of $3.5m/s$ and $2m/s$ for the high heat deposition and the low heat deposition regions respectively. The total volumetric flow rate in the inlet pipe is $11.52m^3/h$ and realizable $k-\epsilon$ turbulence model with standard wall functions was used to simulate the conjugate heat transfer problem. The operational pressure in this study was maintained at $4bar$ and it was reported that the peak temperatures reached in the cooling system is always less than the boiling temperature of the water at the given pressure.

To arrive at the final design of the cooling system of the BDF target was a very challenging aspect of the overall design study. The straight channels between the different target blocks is simpler from the design and manufacturing point of view. In addition to that, the straight channels result in less pressure drop and temperature rise from inlet to the outlet of the cooling system. However more volumetric rate flow rate of the coolant is required in such cases with uneven distribution of the coolant in various channels. Due to this reason, serpentine channels are more favourable because they ensure equal mass flow rate in all the channels of the cooling system. In addition to that, serpentine channels offer better mixing and higher heat transfer coefficients which is favourable for the heat transfer process. Chaitanya et al. [8] investigated the flow and heat transfer of laminar flow in the serpentine channels, numerically and experimentally. Effects of different parameters like the bend angle, straight length before bend and the curvature were studied on the pressure drop and the heat transfer. It was reported in their study that the serpentine configurations with smooth bends offers lower pressure drop and the highest heat transfer enhancement was obtained for 90° bend angle. A similar study to analyze the effect of bend angle and curvature ratios of the pressure drop for different laminar Reynolds number has been done by Maharydrayya et al [33]. Before initiating the present study on the cooling system of the final BDF target, the cooling system of the protoype [12] of the same facility has been studied earlier using the serpentine flow configuration. In this study water is used as the coolant with an operational pressure of $20bar$ and the average velocity in the channels to be around $4m/s$. As mentioned earlier, the serpentine type of design is used in this cooling system with the channel thickness of $5mm$. The total pressure drop was reported to be around $2.5bar$ with an average surface heat transfer coefficient of about $16000W/m^2K$.

All the literature described above were studied and the design of the present cooling system of the final BDF target was established. However, as the flow in the channels of the final BDF target is highly turbulent in nature, therefore it's important to investigate some aspects of the channel flow like the dependence of friction factor and heat transfer coefficient on the Reynolds number and the mean velocity profile in the log-law layer [21], [32], [10], [26]. The effect of different Reynolds number on the friction factor for smooth and rough wall has been extensively studied by researchers both, numerically [5], [32], [30], [25] and experimentally [38], [16], [19]. The DNS simulations of fully developed turbulent flow in a channel for the turbulent Reynolds number Re_τ = 180, 395 and 590 was performed by Moser et al. [32] and the mean velocity in the boundary layer was plotted. The effects of the low Reynolds number was not observed in the higher Reynolds number simulations. Maurer et al. [16] studied the effect of fully developed turbulent flow with and without heat transfer on the friction factor. An equation which accurately predicts the change in friction factor was developed for both

heating and cooling. Wei et al. [38] conducted the laser-Doppler anemometer (LDA) velocity measurements for a range of Reynolds number from 3000 to 40000 to investigate the inner scaling laws. Dean [30] studied the dependence of skin friction coefficient in two dimensional rectangular duct where the C_f and the center-line velocity were accurately described for the range of Reynolds number in between 6000 and 600000 by different empirical relationships. Dirker et al. [17] studied the convective heat transfer correlations for different Reynolds number and the results for different annular diameter ratios were reported. McKeon et al. [5] developed a new friction factor relationship for the fully developed pipe flow for the range of Reynolds number from 31×10^3 to 35×10^6 which predicts all the data within 1.4%.

The effect of different channel flow velocities on the heat transfer coefficient is studied by Junjia et al. [20] where, for a pipe diameter of $12mm$, and a channel velocity of $5m/s$ the HTC as high as $18000W/m^2K$ was reported. Nallasamy [23] studied different turbulence models and their application for the internal flows which is very important for the present thesis. Based on all these literature studies, a very robust and reliable numerical model for the cooling system of the BDF target was developed which is presented in the subsequent sections.

2

Target cooling system

As explained earlier, because of the high power deposition in the target blocks due to the impact of the proton beam, the continuous cooling of the whole system is of vital importance to minimize the thermal stresses. For this purpose, a new cooling circuit was designed which is explained in the next section.

2.1. Cooling system design

Figure 2.1 shows the computational domain of the cooling circuit in three dimension with light grey and dark grey blocks showing the TZM and W targets respectively. The flow pattern inside the domain is shown in figure 2.2 which is a 2D section of figure 2.1 along YZ plane. As can be seen from figure 2.2, the flow behaviour inside the cooling domain is serpentine in nature with two parallel water streams of thickness $5mm$ each (indicated by arrows) on each side of the target block. The serpentine designs are favourable for these kind of cooling systems because of less mass flow requirement for achieving similar velocity in all the channels. This design with two parallel streams was finalized because of the following reasons:

- to avoid the blockage of the cooling circuit, which may happen either because of the target material expansion in the axial direction (due to excessive heating) or because of the unwanted debris in the water supply.
- to minimize the temperature rise from inlet to the outlet of the cooling circuit because, for the identical power deposition on the target blocks, more parallel streams in the serpentine configuration means more mass flow rate and hence less temperature rise.
- to minimize the pressure drop from inlet to the outlet of the cooling circuit which comes from the Darcy-Weishbach equation.

To facilitate this serpentine design, 10 blockers of thickness 10 mm each is used alternatively on blocks 2, 4, 6, 8, 10, 12, 14 and 16 as illustrated in the given figure. The inlet and outlet pipe diameter is $50mm$ for the numerical simulations (which may be different in the final design phase) and the cooling manifold has a height of $20mm$ (which is again a design parameter). The flow in the manifold is not of much interest because the circumferential surface of the target blocks will not receive direct beam impact.

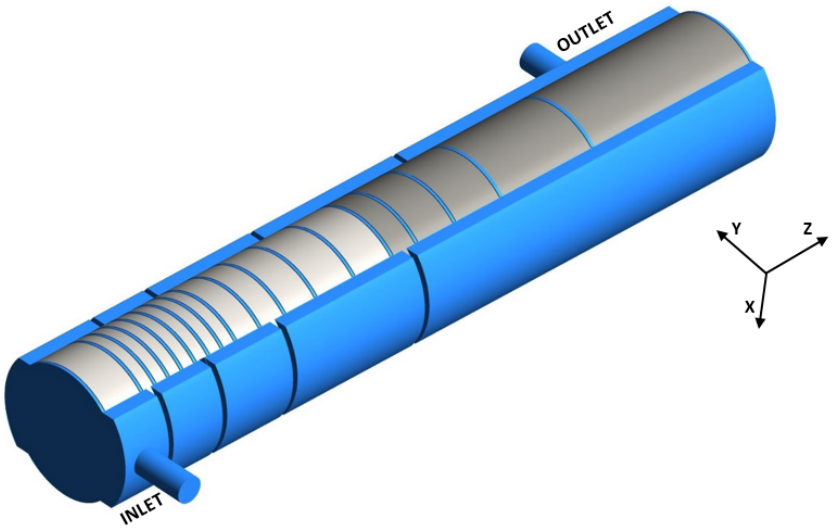

Figure 2.1: ***3D model of the BDF target cooling system.***

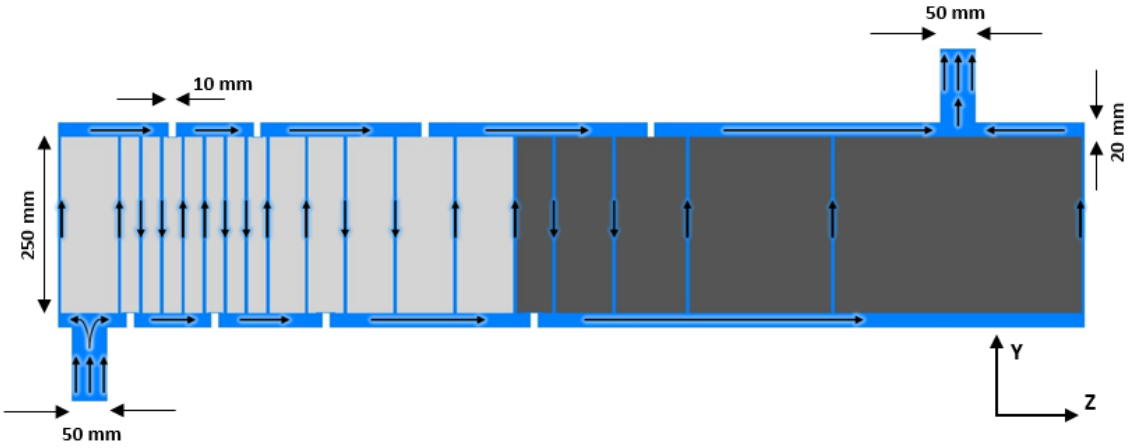

Figure 2.2: ***BDF target longitudinal cross-section. Top view of the cooling circulation path.***

The operational pressure of the cooling system is fixed at $20bar$ and the saturation temperature (T_{sat}) of water at this pressure is $212°C$ which is sufficiently high to avoid boiling. The heat flux at solid-liquid interface increases in the nucleate boiling regime, until the critical heat flux (CHF) is reached (Chapter 10, *Fundamentals of Heat and Mass Transfer* [37]) which is roughly $30°C$ above the saturation temperature (T_{sat}) of water at a particular pressure. The CHF in the present study will reach at around $242°C$, which is far beyond the expected rise of target-water interface temperature in the cooling domain during normal operation (will be shown in section 4) and hence the choice of the operational pressure in the cooling system is substantiated.

Based on the fundamental knowledge of flow dynamics and heat transfer, few analytical calculations were performed in order to get the preliminary idea of the flow of water in the cooling channels and the manifold. The average fluid-solid interface temperature and the average heat transfer coefficient on the wall of the cooling channel was also calculated which is shown in the subsequent section. The properties of water was taken constant and are tabulated as below:

Table 2.1: ***Properties of water at normal temperature and pressure***

Density, ρ [kg/m^3]	998.2
Specific heat, C_p [J/kg.K]	4182
Thermal conductivity, k [W/m.K]	0.6
Dynamic viscosity, μ [kg/m.s]	0.001003
Prandtl number, Pr [-]	7

2.2. Analytical calculations

The water velocity has been limited by design to 5 m/s in the channels, in order to avoid undesired erosion effects on the tantalum-tungsten surface. It is known that other spallation sources such as ISIS at RAL (UK) use high water velocities up to 10 m/s in tantalum-cladded targets such as TS1. At the present design stage of the BDF target, it has been considered to apply a safety factor 2 with respect to this value in order to ensure the safe operation of the target. However a comparative study will be done later in this section with the channel velocities of 1, 2.5, 7.5 and 10 m/s as well. From figure 2.2, as we can see that after water enters the cooling domain from inlet, it gets bifurcated into two streams of parallel channels passing adjacent to the first target blocks. A zoomed part of figure 2.2 having two cooling channels and the inlet is shown in figure 2.3. Owing to serpentine nature of flow, the same pattern is followed in the later section of the domain as well which means that the sum of mass flow rate of the water in any two cooling channel is similar which is equivalent to the inlet mass flow rate. However, in the last part of the cooling domain, three channels are in parallel and therefore the average velocities in these channels will be less than $5m/s$.

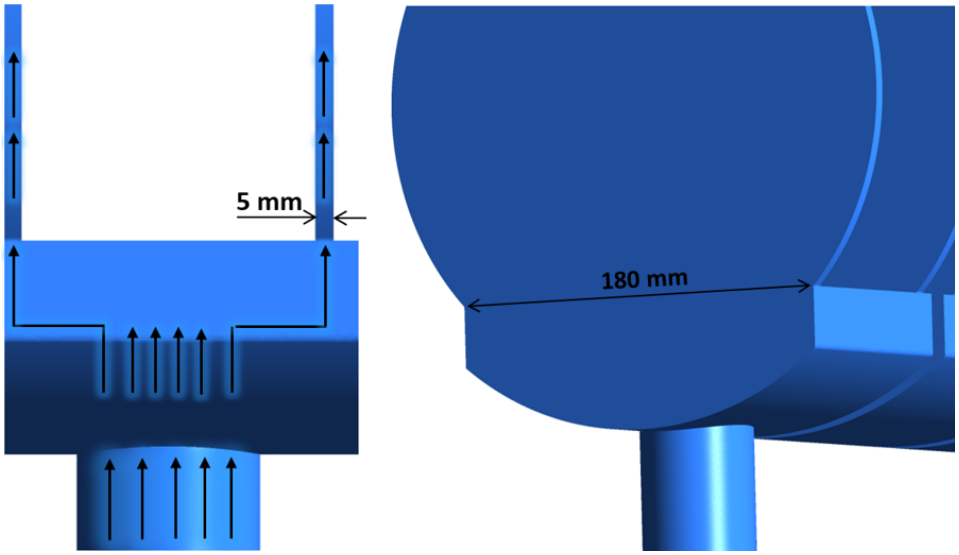

Figure 2.3: ***Cooling circuit's channel dimension and flow bifurcation.***

Using the principle of mass conservation, the inlet mass flow rate can be calculated as follows:

$$\dot{m} = 2\rho A v_c \tag{2.1}$$

where ρ is the density of water, v_c is the velocity of water in the channel and A is the cross-section area of the cooling channels which can be simplified as the rectangular cross-section with the channel thickness of $5mm$ and the width of $180mm$. Using this information, the mass flow rate can be calculated as below:

$$\dot{m} = 2 \times 998.2 \times 0.18 \times 0.005 \times 5 \approx 9kg/s \tag{2.2}$$

From table 1.1 we know that the average beam power deposited on the target is 305 kW. Using the energy balance, the temperature rise of water from the inlet to the outlet of the flow configuration can be found out using equation 2.3:

$$Q = \dot{m} C_P \Delta T \tag{2.3}$$

$$\Delta T = \frac{Q}{\dot{m} C_p} = \frac{305000}{9 \times 4182} \approx 8.12^{\circ}C \tag{2.4}$$

We are primarily focused in resolving the flow and heat transfer in the channels (and not in the manifolds) because of two reasons:

- The beam impacts along the axial direction of the target blocks and hence the maximum energy deposition in all the blocks will be along the longitudinal and radial direction (not along the circumferential direction).
- The conjugate heat transfer is primarily dependent on the flow speed and the contact area (between solid and fluid) and because the average velocity of the water in the channels is approximately 5 times more than in the manifold and hence we can safely assume that the circumferential side of the target blocks won't dissipate much heat into the water.

As mentioned earlier, because of design parameter we are interested to obtained an average velocity of $5m/s$ in the channels (however, as explained earlier, the last three channels of the cooling configuration will have lower velocity) of the cooling circuit. Using this information and the concept of mass conservation, we can calculate the inlet velocity. As shown in figure 2.3, the water stream incoming from inlet gets bifurcated into two channels and hence the mass conservation law can be applied between the inlet and two channels. The diameter of the inlet pipe in the numerical model is $50mm$, as explained in section 2.1. The inlet area to the channel can be simplified as a rectangular orifice of length 180mm and width 5mm (shown in figure 2.3) and using the mass conservation, we get:

$$(\text{Mass flow})_i = 2 \times (\text{Mass flow})_c \tag{2.5}$$

$$\rho \times A_i \times v_i = 2 \times \rho \times \mathrm{A}_c \times v_c \tag{2.6}$$

$$v_i = \frac{2 \times A_c \times v_c}{A_i} = \frac{2 \times 0.18 \times 0.005 \times 5}{\pi \times 0.25^2} \tag{2.7}$$

$$\Rightarrow v_i \approx 4.58 m/s \tag{2.8}$$

The indices i and c indicates inlet and channel respectively. Using the velocity of water in channel, we can calculate the average Reynolds number inside the channel as follows:

$$Re_c = \frac{\rho \times v_c \times D_H}{\mu} \tag{2.9}$$

where D_H is the hydraulic diameter of the channel and can be calculated as:

$$D_H = \frac{4 \times A_c}{P_c} = \frac{4 \times 0.005 \times 0.18}{2 \times (0.005 + 0.18)} = 0.00973mm \tag{2.10}$$

Using this value in equation 2.9 and substituting the value for water properties, we get:

$$Re_c = \frac{998.2 \times 5 \times 0.00973}{0.001003} \Rightarrow Re_c = 48415 \tag{2.11}$$

This shows that the flow in the channels is highly turbulent in nature. The HTC at the fluid-solid interface can be analytically calculated using the following expression:

$$h = \frac{Nu \times k}{D_H} \tag{2.12}$$

where k is thermal conductivity of the water, D_H is the hydraulic diameter of the channel and Nu is the Nusselt number. Several convection correlations can be used to calculate the value of Nu for turbulent flow in a channel. After some literature survey [37], it was concluded that assuming flow over smooth surface, either Dittus-Boelter or Gnielinski equation can be used (however Gnielinski equation gives higher level of accuracy, which will be shown in the subsequently). The Dittus-Boelter [31] equation can be written as:

$$Nu_D = 0.023 Re_D^{4/5} Pr^n \tag{2.13}$$

which is valid for, $0.6 \leq Pr \leq 160$, $Re_D \geq 10,000$ and $\frac{L}{D} \geq 10$. The n in the equation 2.13 is 0.4 if solid temperature is more than the liquid temperature and 0.3 liquid temperature is more than the solid temperature. The Gnielinski equation [40] can be written as:

$$Nu_D = \frac{(f/8)(Re_D - 1000)Pr}{1 + 12.7(f/8)^{1/2}(Pr^{1/3} - 1)} \tag{2.14}$$

which is valid for, $0.5 \leq Pr \leq 2000$ and $3000 \leq Re_D \leq 10^6$. The f in the above equation is the friction factor which can be calculated using Petukhov relationship [6] as given in equation 2.15.

$$f = \left(0.79\ln(Re_D) - 1.64\right)^{-2} \quad \text{valid for} \quad 3000 \leq Re_D \leq 5 \times 10^6 \tag{2.15}$$

or by using the Blasius relationship, as given below:

$$f = 0184 Re^{-0.2} \quad \text{valid for} \quad Re_D \geq 5 \times 2 \times 10^4 \tag{2.16}$$

Using equation 2.15 and the value of Re_D from equation 2.11, the friction factor in the channel is found out to be $f = 0.021$. The Prandtl number of water is assumed to be constant for the flow and it's value is given in table 2.1. Using the values of f, Re_D and Pr, in equation 2.13 and 2.14 we can calculate the Nu_D whose values are given below:

$$Nu_D = 280 \quad \text{(using Dittus-Boelter equation)} \tag{2.17}$$

$$Nu_D = 320 \quad \text{(using Gnielinski equation)} \tag{2.18}$$

It is recommended [37] to use the value of Nu_D from Gnielinski equation if the higher level of accuracy is desired and therefore using the value of Nu_D from 2.18 in equation 2.12 we can get the value of HTC:

$$h = \frac{320.6}{0.00973} \quad \Rightarrow \quad h = 19,732 W/m^2K \tag{2.19}$$

The high HTC value calculated using the above expression is attributed to the large velocity in the channel which will be validated subsequently. As mentioned earlier in this section, a comparative analytical study was also done considering $1m/s$, $2.5m/s$, $7.5m/s$ and $10m/s$ as the average channel velocity. Table 2.2 compares the various results for different channel velocities. As can be seen from the table, the temperature rise from inlet to the outlet of the cooling domain is $40.6°C$ and $16.24°C$ for cases 1 and 2 respectively however as par the design parameter, the temperature rise should remain below $10°C$. With such a temperature rise in case 1 and 2, the solid-liquid interface temperature may reach beyond the nucleate

boiling regime which is not desirable and hence the channel velocities of $1m/s$ and $2.5m/s$ are not suitable.

In case 4 and 5, even though the temperature rise is within the stipulated limit and HTC values are high enough, which is imperative to dissipate maximum heat from the target blocks but due to very high velocity of water (7.5 and 10 m/s) in channels of width $5mm$ erosion and corrosion may take place which is again not a desirable condition for the experiment. In addition to that, high velocity in the channels will lead to high pressure drop which will be shown in section 4.2. Even though the channel velocity of $5m/s$ is the design parameter for this study, but this comparative analysis shows that why case 1, 2, 4 and 5 are not desirable.

Table 2.2: ***Comparison of various analytical results with the channel velocity***

$Case\ No.$	v_c	$\dot{m}$	ΔT	f	Nu (using 2.14)	HTC (using 2.14)
1	1	1.8	40.6	0.031	77.1	4754.63
2	2.5	4.5	16.24	0.025	175.29	10809.61
3	5	9	8.12	0.021	320.04	19736
4	7.5	13.5	5.4	0.019	454.2	28009.24
5	10	18	4.06	0.018	582.2	35903.1

The analytic calculations has already given us a broad idea about the flow and heat transfer characteristics in the cooling circuit and specifically in the cooling channels. In-spite of that, an extensive CFD study of the full scale cooling system was needed to be done mainly because of the complexity of the flow in the turbulent regime and to resolve the flow and heat transfer in the boundary layer of the channels. In conjugate heat transfer problems (like the present one), the heat being transmitted from solid to the liquid is highly dependent on the thermal boundary layer and therefore very sophisticated turbulence models (like $k-\omega$ SST or Realizable $k-\epsilon$ with enhanced wall treatment) must be used to resolve the boundary layers. A commercial CFD code, Ansys FLUENT was used to perform the extensive 3D turbulence modeling of the flow configuration. The mathematical formulation of the Reynolds Averaged Navier Stokes (RANS) equation and the boundary conditions in addition to the methodology used to import the energy map for the target blocks is explained in section 3.

3

Mathematical modeling

This chapter describes the flow governing equations used to solve the numerical model, their discretisation and the solution methodology. The flow behaviour of water in the cooling system is assumed to be incompressible and Newtonian in nature. Non-uniform heat deposition map is imposed on the target blocks. As the *Reynolds number* of the flow in the cooling channels is around 48000, hence the Reynolds-averaged Navier-Stokes (RANS) modeling is being done to resolve the flow and heat transfer phenomenon near the walls of the channels. With this information, the flow and energy governing equations to solve the problem can be written which is elucidated in the subsequent section.

3.1. Governing equations

The commercial CFD code, Fluent is used for solving the conjugate heat transfer turbulent problem which uses the conservation equations for mass and momentum as given below:

Mass conservation equation

$$\frac{\partial \rho}{\partial t} + \nabla \cdot (\rho \overline{v}) = 0 \tag{3.1}$$

$\bar{v}$ in the above equation is the velocity field.

Momentum conservation equation

$$\frac{\partial}{\partial t}(\rho \overline{v}) + \nabla \cdot (\rho \overline{v}\overline{v}) = -\nabla p + \nabla \cdot (\bar{\bar{\tau}}) + \rho \overline{g} + \overline{F} \tag{3.2}$$

p and $\bar{\bar{\tau}}$ in the above equation is the static pressure and the stress tensor, which can be written as:

$$\bar{\bar{\tau}} = \mu\left[(\nabla \overline{v} + \nabla \overline{v}^T) - \frac{2}{3}\nabla \cdot \overline{v} I\right] \tag{3.3}$$

where μ is the molecular viscosity and the second term is neglected for the present case. No gravitational body force and the external body forces are imposed in the present case and hence the second last and the last term in equation 3.2 are neglected as well.

Energy equation

$$\frac{\partial}{\partial t}(\rho h) + \nabla \cdot \left[\rho \overline{v} h\right] + \nabla \cdot \left[k_{eff} \nabla T + (\overline{\overline{\tau_{eff}}} \cdot \bar{v})\right] + S_h \tag{3.4}$$

where h is the enthalpy of the system, T is temperature and $k_{eff} = k + k_t$ is the effective conductivity, where k_t is the turbulent thermal conductivity. The $\nabla\cdot(\overline{\tau_{eff}}\cdot\vec{v})$ term is neglected for the present analysis because of the incompressible nature of the flow. S_h is the volumetric heat sources term where the heat deposition map will be added to study the impact of proton beam on the target blocks. h, which is the enthalpy of the system can be written as:

$$h = \int_{T_{ref}}^{T} C_p dT \tag{3.5}$$

where T_{ref} is the reference temperature, taken as $300K$ in the present case.

3.2. RANS turbulence modeling

In most of the industrial problems, resolution of the smallest length scales (Kolmogorov scale) is not required as it is computationally expensive. That's why RANS turbulence modeling is the most favourable approach till date, to solve the practical engineering problems. In this approach, the solution variable, for example the velocity components can be written in the following form:

$$u_i = \overline{u_i} + \tilde{u_i} \tag{3.6}$$

where $\bar{u_i}$ and $\tilde{u_i}$ are the average and fluctuating components. Scalar quantities like pressure and energy can be treated in the similar way. Using these variable in equations 3.1 and 3.2 and taking the ensemble average, an additional term is obtained in the ensemble-averaged momentum equation, known as Reynolds stress which can be written as:

$$\text{Reynolds stress} = -\rho\overline{u_i' u_j'} \tag{3.7}$$

This term must be modeled for the closure of the ensemble-averaged momentum equation. Several RANS turbulence models can be used to model the Reynolds stress term, however to solve the conjugate heat transfer problem in the present case, $k-\omega$ SST (shear stress transport) model was used because of it's ability to solve the internal turbulent flow problems with the better prediction of adverse pressure gradient boundary layer flows and separation. In addition to that, this model can resolve the flow near the wall region and in the far-field zones as well. The conservative form of transport equation for the $k-\omega$ SST [24] model, as used in $ANSYS$ Fluent [2] is given as below:

Turbulent kinetic energy

$$\frac{\partial}{\partial t}(\rho k) + \frac{\partial}{\partial x_i}(\rho k u_i) = \frac{\partial}{\partial x_j}\left(\Gamma_k \frac{\partial k}{\partial x_j}\right) + \tilde{G_k} - Y_k + S_k \tag{3.8}$$

where, $\tilde{G_k}$ and Y_k represents the generation and dissipation of turbulent kinetic energy, k and S_k is the user defined source term.

Specific dissipation rate

$$\frac{\partial}{\partial t}(\rho\omega) + \frac{\partial}{\partial x_i}(\rho\omega u_i) = \frac{\partial}{\partial x_j}\left(\Gamma_\omega \frac{\partial \omega}{\partial x_j}\right) + \tilde{G_\omega} - Y_\omega + S_\omega + D_\omega \tag{3.9}$$

where, G_ω and Y_ω represents the generation and dissipation of specific dissipation rate, ω and S_k and D_ω represents the user defined source term and the cross diffusion term respectively. Γ is the effective diffusivity and it's modeling is performed as shown below:

$$\Gamma_k = \mu + \frac{\mu_t}{\sigma_k} \tag{3.10}$$

$$\Gamma_\omega = \mu + \frac{\mu_t}{\sigma_\omega} \tag{3.11}$$

where, σ_k and σ_ω are the turbulent $Prandtl$ numbers for k and ω respectively and μ_t is the turbulent viscosity.

3.3. Solution methods and Discretization

This section will elucidate the spatial and temporal discretization schemes used in the present study. The way of importing energy mapping to the target blocks and adding it as the source term in the energy equation is explained in the appendix B.

3.3.1. Spatial discretisation using FVM

A control-volume based technique is used to discretize the scalar transport equations in $ANSYS$ Fluent [2] which are subsequently converted in the form of algebraic equations and are solved numerically. A discrete equation is obtained by integrating the transport equation for a scalar quantity ϕ, at each control volume of the domain as shown below:

$$\int_V \frac{\partial \rho\phi}{\partial t} dV + \oint \rho\phi\overline{v} \cdot d\overline{A} = \oint \Gamma_\phi \nabla\phi \cdot d\overline{A} + \int_V S_\phi dV \tag{3.12}$$

where, ρ is density, $\overline{v}$ is velocity vector, $\overline{A}$ is surface area vector, Γ_ϕ is the diffusion coefficient for the quantity ϕ, $\nabla\phi$ is the gradient of ϕ and S_ϕ is the source term per unit volume. Equation 3.12 is solved in the whole computational domain for each cell and then it's summed up to give the final solution. The discretized form of equation 3.12 can be written as:

$$\frac{\partial \rho\phi}{\partial t} V + \sum_f^{N_{faces}} \rho_f \overline{v_f} \phi_f \cdot \overline{A_f} = \sum_f^{N_{faces}} \Gamma_\phi \nabla\phi_f \cdot \overline{A_f} + S_\phi V \tag{3.13}$$

where N_{faces} is the number of fces enclosing cell, ϕ_f is the vlue of ϕ convected through face f, $\rho_f \overline{v_f} \cdot \overline{A_f}$ is the mass flux through the face, $\overline{A_f}$ is the area if the face f, $\nabla\phi_f$ is the gradient of ϕ at face f which is calculated by using the least square cell based method and V is the cell volume. A typical 2D control volume used to illustrate the discretization of the scalar transport equation is shown in figure 3.1.

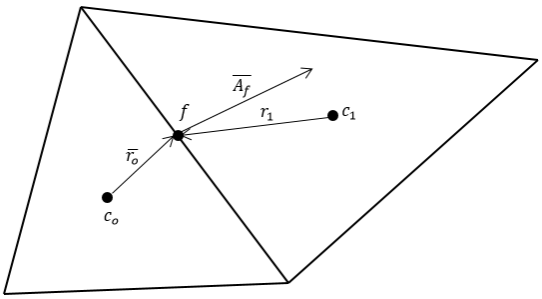

Figure 3.1: ***A typical 2 dimensional control volume***

As shown in figure 3.1, the discrete values of the scalar quantity ϕ is stored at the cell centers (c_o and c_1) which are interpolated to get the corresponding values of the scalar quantity at the face, f which in turn are used in equation 3.13. In the present work, the turbulent kinetic energy, k and the specific dissipation rate, ω equations are interpolated using the first order upwind scheme whereas the second order upwind scheme is used for the interpolation of momentum and energy equations.

First Order Upwinding

In this case the solution obtained at cell-center (ϕ) is set equal to the face values (ϕ_f), as a result of which the first order accuracy is obtained.

Second Order Upwinding

Here the values at the cell faces are calculated using a multidimensional linear reconstruction approach [7] which provides the second order accuracy in the solution. In this case, the ϕ_f is calculated using the following expression:

$$\phi_{f,SOU} = \phi + \nabla\phi \cdot \bar{r} \tag{3.14}$$

where $\bar{r}$ is the displacement vector from the upstream cell centroid to the face centroid. The gradient $\nabla\phi$ is calculated using the least square cell based spatial discretization method.

SIMPLE algorithm

The pressure-based segregated solver (PBSS) is used in this study which is based on the predictor-corrector approach and uses the projection method [3] where the continuity and the momentum equations are used to derive the pressure equation. As the governing equations are nonlinear in nature and hence an iterative algorithm named SIMPLE (Semi-Implicit Method for Pressure-Linked Equations), as shown in figure 3.2, which was developed by Patankar and Spalding [28], is solved until the desired convergence is reached.

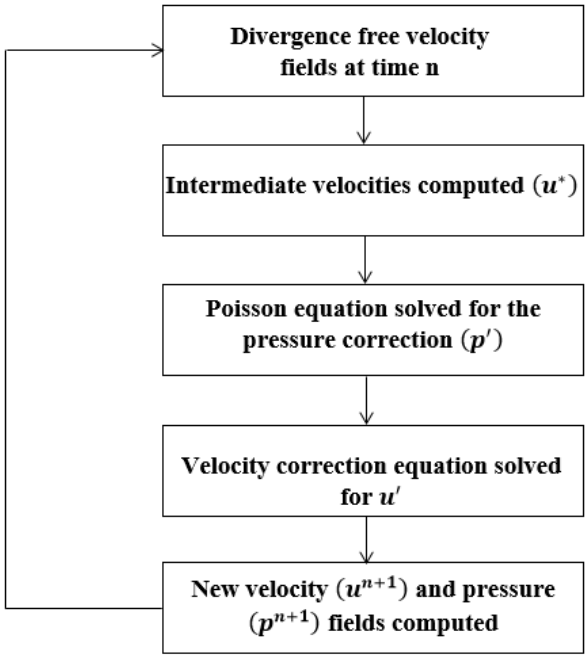

Figure 3.2: ***Algorithm for pressure based segregated solver (SIMPLE)***

Under-relaxation

Under-relaxation of variables is the method of slowing down the change of ϕ during each iteration. This is in the following manner:

$$\phi_{new} = \phi_{old} + \alpha\Delta\phi \tag{3.15}$$

where ϕ_{new} and ϕ_{old} are the new and old values of the variable, $\Delta\phi$ is the change and α is the under-relaxation factor (URF) whose values varies between 0 to 1. Under-relaxation of the variables is necessary because of the non-linearity of the governing equations which usually leads to divergence if the mesh is skewed or turbulence model is used. Divergence in the

solution may arise due to other reasons as well, but URF is used to stabilize the convergence process but usually slows it down. The under-relaxation of equations is performed in the following way:

$$\frac{a_p \phi}{\alpha} = \sum_{nb} a_{nb} \phi_{nb} + b + \frac{1-\alpha}{\alpha} a_p \phi_{old} \tag{3.16}$$

Over-relaxation ($\alpha > 1$) of the variables is done to speed up the convergence process but usually leads to divergence for the complex problems.

3.3.2. Time integration

The temporal term in equation 3.13 can be discretized either explicitly (n^{th} time level) or implicitly ($(n+1)^{th}$ time level). All the problems in the present work are solved using first order implicit schemes and hence the other temporal discretization methods will not be discussed here, however for more information readers are advised to refer [2]. The implicit time integration scheme can be written as:

$$\frac{\phi^{n+1} - \phi^n}{\Delta t} = F(\phi^{n+1}) \tag{3.17}$$

$$\phi^{n+1} = \phi^n + \Delta t F(\phi^{n+1}) \tag{3.18}$$

where, ϕ is a scalar quantity, $n+1$ is the value of the next time level ($t + \Delta t$), n is the value at the current time level (t) and F is a function which incorporates any spatial discretization. The value of ϕ^{n+1} in a given cell is related to ϕ^{n+1} in the neighbouring cells through $F(\phi^{n+1})$. The implicit time integration scheme is unconditionally stable with respect to the time step size. Using this information, the equation 3.12 can be written as:

$$\int_V \frac{\partial \rho \phi}{\partial t} dV + \oint \rho^{n+1} \phi^{n+1} v^{n+1} \cdot d\overline{A} = \oint \Gamma_\phi^{n+1} \nabla \phi^{n+1} \cdot d\overline{A} + \int_V S_\phi^{n+1} dV \tag{3.19}$$

The above equation is solved iteratively in Fluent using the algorithm shown in figure 3.3.

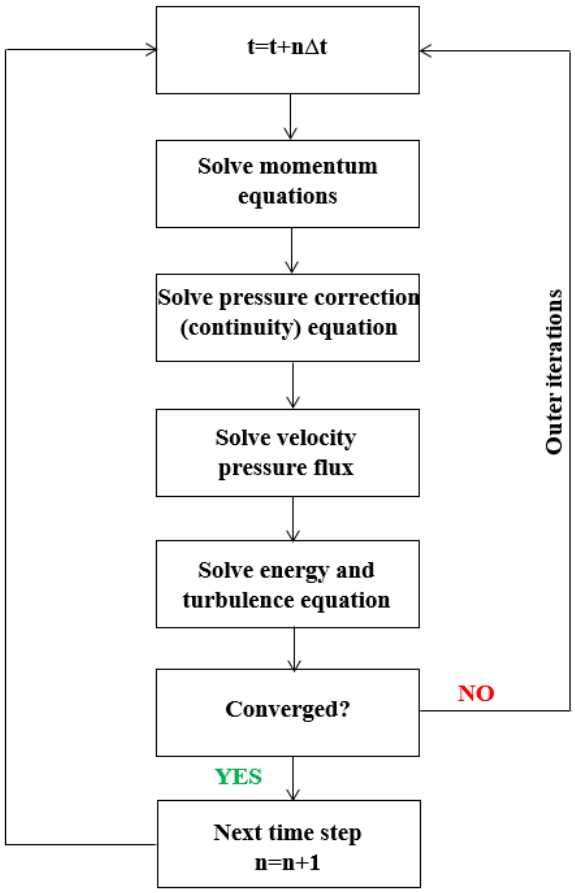

Figure 3.3: ***Algorithm for pressure based segregated solver***

4

Results and Discussions

As the flow in the channels is highly turbulent in nature (Re_D=48415 with the channel velocity of $5m/s$), therefore in order to resolve the wall boundary layers, the $k-\omega$ shear stress transport(SST) model [24] was used because of it's ability to resolve the flow near the wall region and in the core as well. A Neumann boundary condition for pressure was used at the outlet of the domain. No-slip boundary condition was given at the walls of the cooling domain and the target blocks and the coupled boundary condition for temperature is given at the target-water interface. Inlet temperature is maintained at $27°C$. The energy profile distribution in space, which is obtained for each block from the FLUKA [1] MonteCarlo simulations is imported in the ANSYS FLUENT model by using a user defined function (UDF) and is used as a source term in the energy equation, except for the 2D validation case where a constant energy density is given to the each block.

4.1. Validation Cases

As elucidated earlier in section 2, the cooling system being investigated in this study is quite complex because of the unusual design of the cooling channels where the water enters from the circumferential direction. In addition to that even though the serpentine design of the cooling system in the conventional heat exchangers is quite common but in the present work there are two unidirectional channels for initial 16 targets and three unidirectional channels for the remaining part which makes the overall serpentine design. However quite good analytical, numerical and experimental validations were obtained which are explained in the subsequent sections.

4.1.1. 2D analysis of the full scale model

Figure 2.2 illustrates the 2D model of the target and cooling system being investigated which is basically a 2D slice of the figure 2.1 in the YZ plane. A structured mesh with sufficient clustering near the boundary layer region in order to get the y^+ of 1 was used which is shown in figure 4.1. 10 inflation layers were used at the interface which is illustrated in figure 4.1b (this is the zoomed region of figure 4.1a marked by red square in the top-left part). The inlet velocity of $1m/s$ was used to get a velocity of $5m/s$ in the channels which was obtained using mass-conservation principle as shown in equation 2.5. Constant value for energy deposition (as given in figure 1.5) per unit volume was given in all the target blocks. Three different meshes were used with 10, 15 and 20 elements in the cooling channels along the axial direction to study the dependence of final solution on the mesh density. The total number of elements in the mesh for these three cases are 216884, 249429 and 266555 respectively.

[1] http://www.fluka.org/fluka.php

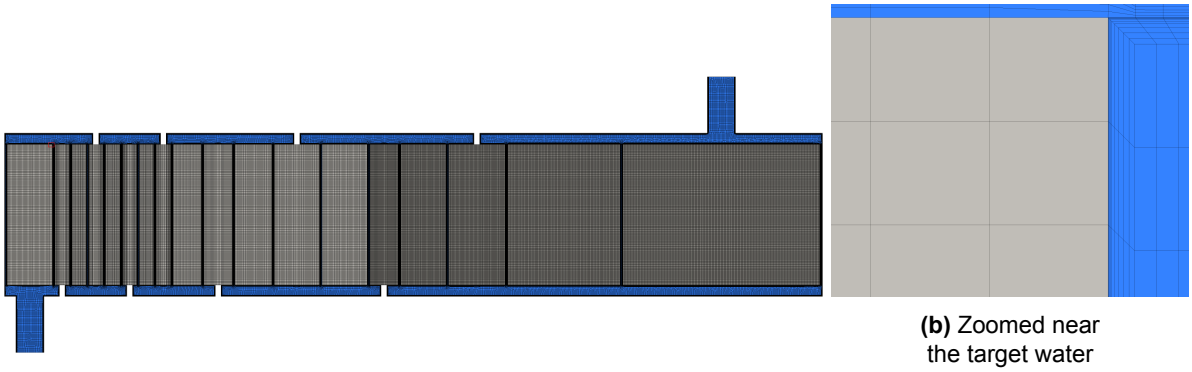

(a) Full assembly

(b) Zoomed near the target water interface

Figure 4.1: ***Computational mesh used for the 2D simulations***

Figure 4.2 and 4.3 shows the velocity contour and the average velocity distribution of water in channels respectively. From the figure it is evident that the average velocity in the first 16 channels is close to $5m/s$ as expected, however for the last three channels the average velocity is lower, because of less mass flow rate passing through those channels. The pressure distribution in the cooling circuit is illustrated in figure 4.4 where it can be seen the the total pressure drop in the domain is around $2bar$.

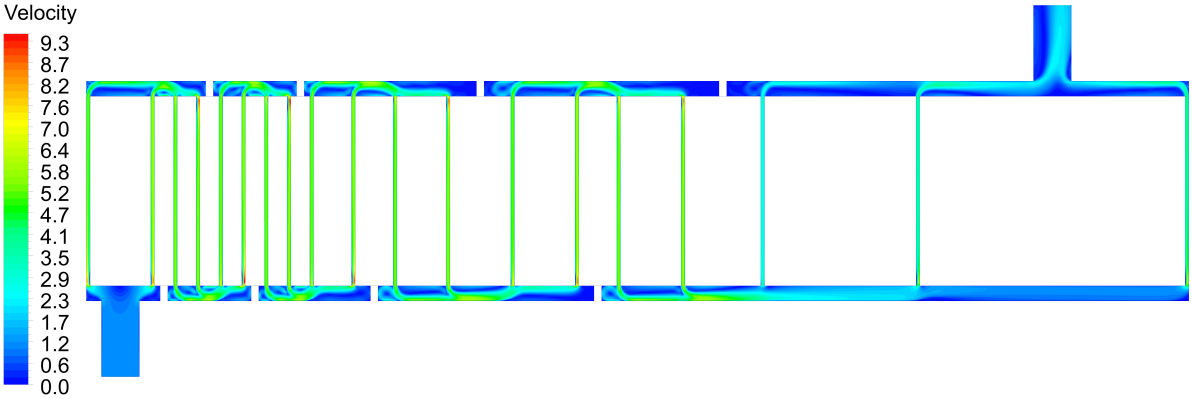

Figure 4.2: ***Velocity contour in the cooling system in the 2D domain.***

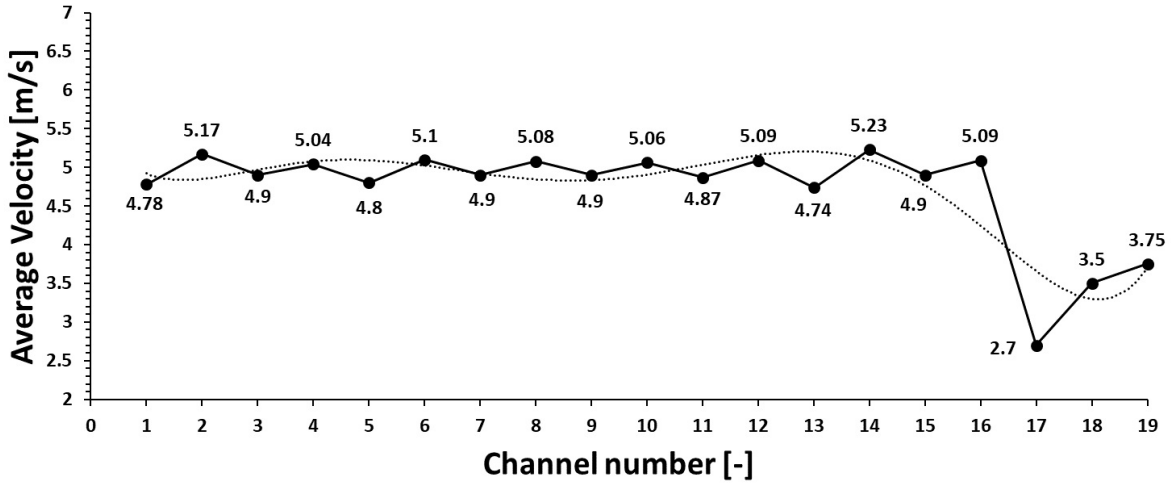

Figure 4.3: ***Variation of average velocities in the channels for 2D simulation with · · · pattern as the trend-line.***

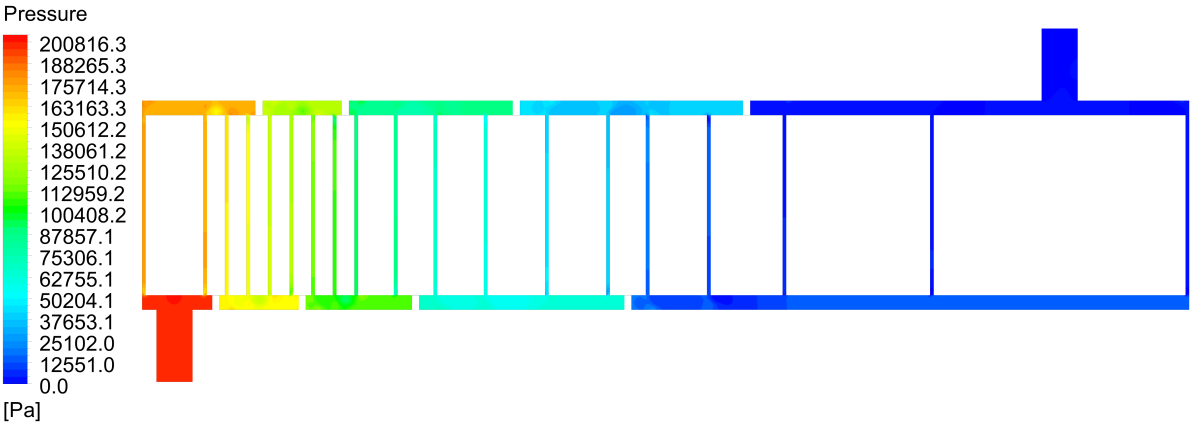

Figure 4.4: ***Pressure distribution in the cooling system in the 2D domain.***

As the cooling channels in this case can be treated as the flow in the rectangular channel and hence Darcy Weisbach equation was used to calculate the pressure drop and was compared with the results obtained from the simulations. The Darcy Weisbach equation, as given in the *Fundamentals of heat and mass transfer* [37] can be written as below:

$$\Delta P = f\frac{\rho\overline{u}^2 L}{2D} \tag{4.1}$$

where ΔP is the pressure drop in the channel, f is the Darcy friction factor (calculated using 2.15), ρ is the density of the fluid, $\overline{u}$ is the average velocity of fluid, L is the length of the channel and D is the hydraulic diameter. The pressure drop using this equation (where $\bar{u}$ was taken from figure 4.3) and that obtained from the simulation for all the channels is plotted in figure 4.5 and a comparative study was done. As can be seen from this figure, three cases are validated against the values of pressure drop obtained using the anaytical calculations and a good match exists. Cases A, B and C are basically pressure drop obtained using three different meshes with 10, 15 and 20 elements respectively in the cooling channels along the axial direction. It can be seen from the figure 4.5 that the values of pressure drop for case B and C are similar and hence it can be concluded that all the results obtained using case B are grid independent.

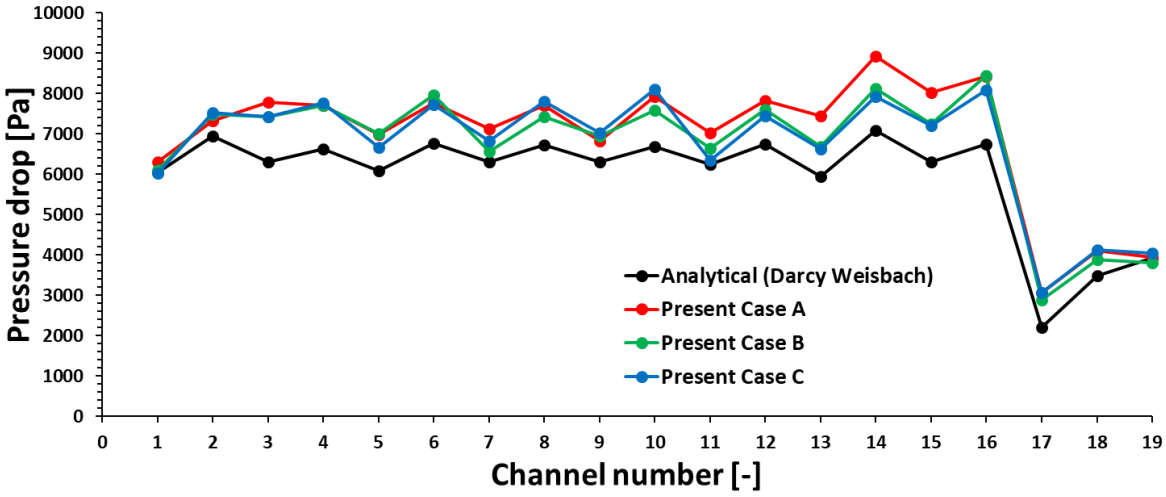

Figure 4.5: ***Comparison of pressure drop in all the 19 channels of the cooling domain between analytical calculations and the 2D simulation. Cases A, B and C represents channels with 10, 15 and 20 elements in axial direction respectively.***

Figure 4.6 shows the temperature distribution in the cooling circuit with the temperature rise found from inlet to the outlet to be around $8°C$. The primary purpose of performing this study is to get the temperature distribution plot in all the target blocks using the numerical simulation and to compare it using the one dimensional conduction equation with heat generation which is given below:

$$\frac{d^2T}{dx^2} + \frac{\dot{q}}{k} \tag{4.2}$$

where $\dot{q}$ is the energy generation per unit volume (as given in figure 1.5 for each block) and k is the thermal conductivity of solid (as given in table 1.3). However, in order to make the one-dimensional approximation of the current 2D model, no heat flux condition must be given at the top and bottom boundaries of all the target blocks. Figure 4.7 shows the temperature distribution in the cooling domain using this condition.

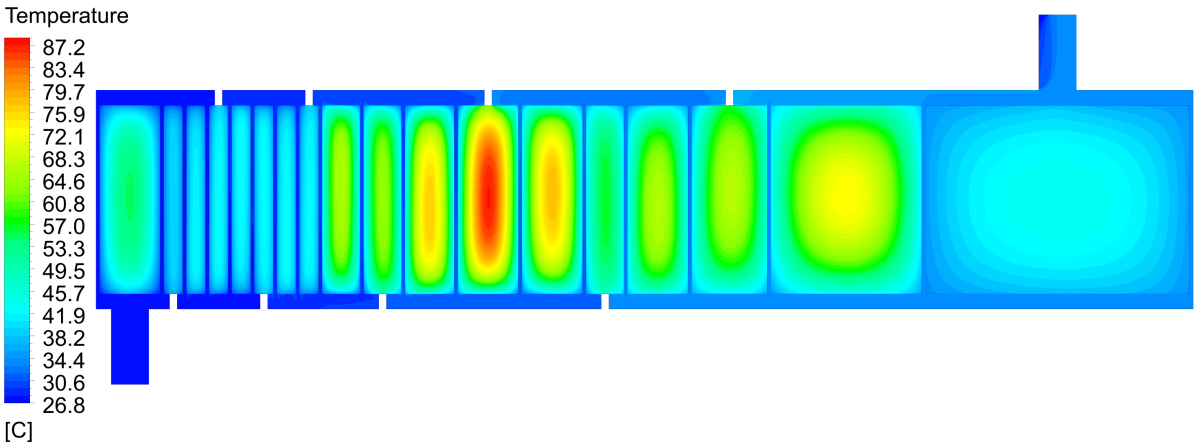

Figure 4.6: ***Temperature distribution in the cooling circuit (Case 1)***

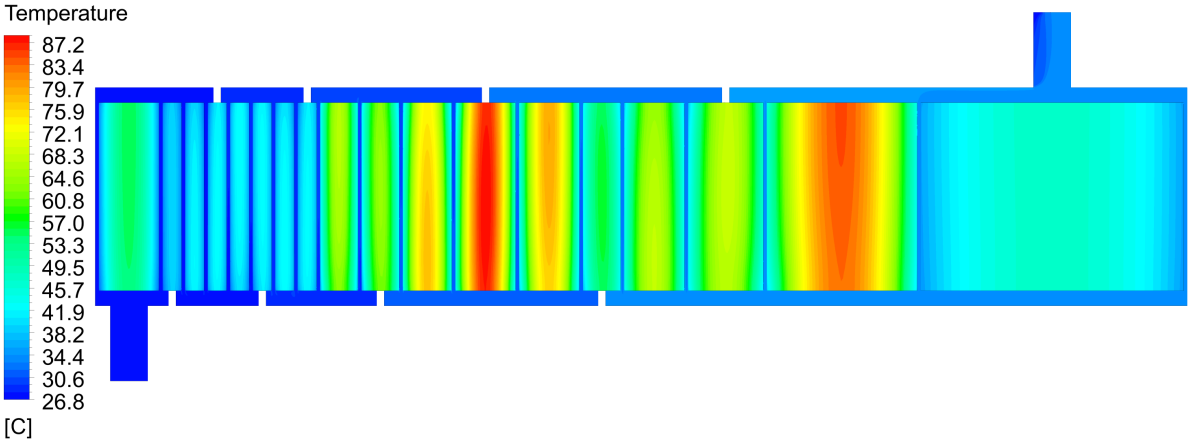

Figure 4.7: ***Temperature distribution in the cooling circuit (Case 2)***

Figure 4.8 shows the comparison of the heat transfer coefficient values obtained using the analytical calculations (as shown in section 2.2) and the numerical simulations. Average velocity in the channels (as shown in figure 4.3) were used to calculate the analytical values of HTC. Two different simulations with no heat flux boundary condition on the top and bottom surface (Case 1) and the coupled boundary condition on all surfaces of the target blocks (Case 2) were performed to plot the HTC. To calculate the analytical value of HTC, the average velocity in the channel was used from figure 4.3.

Even though it's evident from the figure 4.6 that the temperature distribution in the target blocks is non-uniform but it's imperative to elucidate the non-applicability of *lumped capacitance model* for the present case which can be done by calculating the *Biot number (Bi)* for all the blocks. The *Bi* can be written as below:

$$Bi = \frac{hL}{k} \tag{4.3}$$

where h is the heat transfer coefficient (figure 4.8) at the solid-liquid interface, L (=4A/P) is the characteristic length and k is the thermal conductivity of the solid (used from table 1.3). Table 4.1 shows the value of *Biot number* for different target blocks.

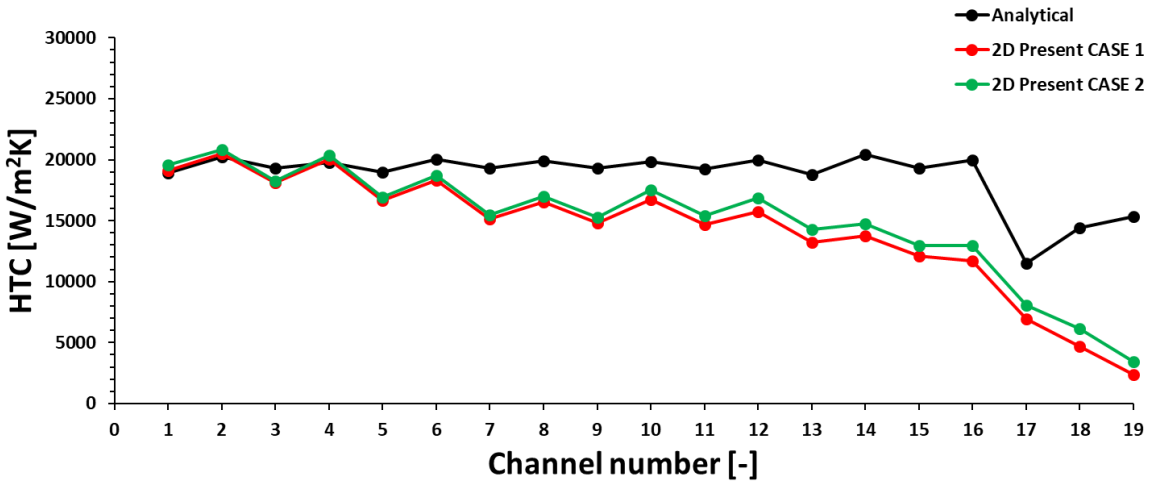

Figure 4.8: ***Comparison between analytical calculations and the numerical simulation for the convective heat transfer coefficient in different cooling channels.***

Table 4.1: ***Biot number for different target blocks***

Target number	Biot number	Target number	Biot number
1 (TZM)	25.6	10 (TZM)	16.8
2 (TZM)	8.5	11 (TZM)	21.1
3 (TZM)	8.2	12 (TZM)	27
4 (TZM)	8.4	13 (TZM)	25.4
5 (TZM)	8	14 (W)	11.8
6 (TZM)	8.4	15 (W)	17.8
7 (TZM)	8.2	16 (W)	23
8 (TZM)	8.4	17 (W)	26.6
9 (TZM)	16.3	18 (W)	58

It can be seen from the table 4.1 that $Bi \gg 1$ for all the blocks and hence the *lumped capacitance model* is not applicable and the temperature inside the target blocks are much different from the surface temperature. The average surface temperature for all the target blocks can be calculated by applying the energy balance to the plane wall as given below:

$$\dot{q} L_h = h(T_s - T_b) \tag{4.4}$$

where L_h is the half length of the target blocks and the other symbols have their usual meaning. Using this expression to calculate the average surface temperature of all the blocks and applying it as the boundary condition in the solution of equation 4.2, the analytical temperature distribution in the blocks can be obtained which is plotted in figure 4.9 along with the results of numerical simulations for the two cases (figures 4.6 and 4.7).

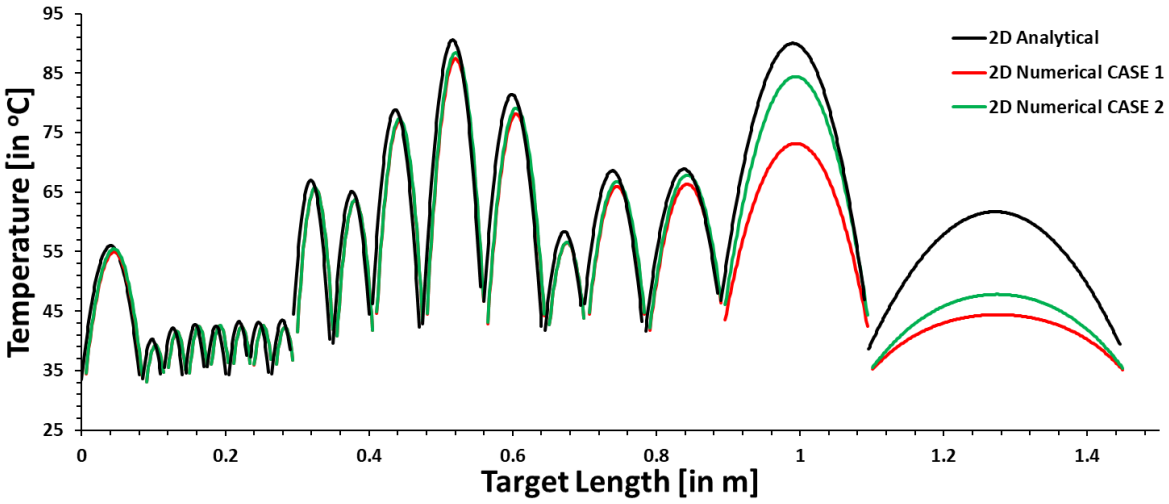

Figure 4.9: ***Comparison of temperature profiles in the target blocks for analytical calculations and the numerical simulation***

Figure 4.9 shows a nice match of temperature profile for the first 16 blocks between analytical calculations and the 2D simulation results. For the remaining 2 blocks, even though a similar trend between analytical and numerical solution is obtained but the maximum temperature in the blocks is different because the thickness of those blocks ($200mm$ and $350mm$) is comparable to their height ($250mm$) and hence 1D approximation doesn't hold good. In addition to that we can see that the results for Case 2 is more closer to the analytical solution as compared to the results of Case 1 because Case 2 is much close to 1D approximation because o the no heat flux boundary condition given on the top and bottom wall of the target blocks.

From this section it can be concluded that the turbulence model, mesh size and the boundary conditions being used for the 2D model (which is a section of the 3D model in the YZ plane)

gives results which are comparable with the analytical calculations and hence it can be stated that the numerical model being developed is quite robust.

4.1.2. 3D analysis of the single channel model

In this test case, single 3D channel is considered as shown in figure 4.10 which is a part of one of the 19 channels as illustrated in figure 2.1. The inlet, outlet and other nomenclature of this cooling channel assembly in addition to the computational mesh is shown in figure 4.10a. Figure 4.10b illustrates the inflation layers near the boundary region in the channel and the manifold. This case is investigated to study the flow behaviour of water in the cooling channels and hence the energy equation was not solved. As shown in figure 4.10b, 12 inflation layers are used in the boundary layer with $y^+ = 1$ and 10 elements are used along the axial direction in the channel. The final mesh is structured with hexahedral elements in the core and the wedge elements in the inflation layer and the total number of elements in the mesh is 391474.

This model is simulated for various inlet velocities like 4.58, 5, 6, 7, 8, 9 and $10 m/s$. Figure 4.11 illustrates the velocity contour, streamlines and the pressure contour in the cooling channel for the inlet velocity of $4.58 m/s$. As can be observed from the velocity contour of this figure, the flow in the cooling channel can be simplified to the general case of flow in a rectangular channel because of the presence of strong re-circulation zones (blue coloured contour on the left and right side of the domain) due to which the average velocity in these regions tends towards zero.

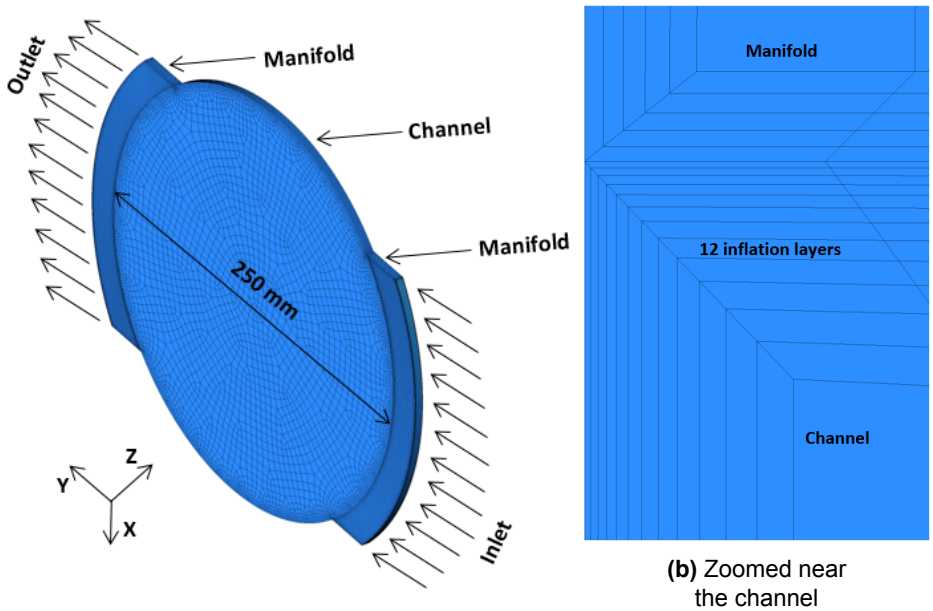

(a) Full assembly

(b) Zoomed near the channel manifold interface

Figure 4.10: ***Cooling channel domain and the computational mesh used for the 3D simulations of single channel study***

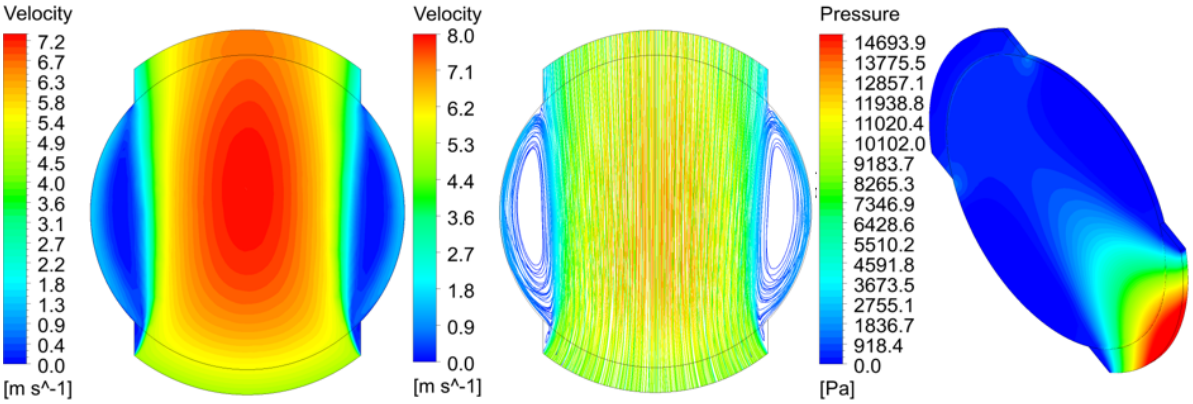

Figure 4.11: ***Velocity contour, streamlines and the pressure contour in the cooling channel for inlet velocity of*** $4.58m/s$

Figure 4.12 shows the velocity profile in the channel along the axial direction at different locations in the Y direction. The brown coloured plot in this figure which represents the velocity profile is taken at $Y = 0$, which is the entrance of the channel. As the Y location is increased towards the center of the channel, the velocity profile starts to become fully developed which can be seen from the locations like $Y = 105$, 115 and $125mm$. The shape of the velocity plot is flattened from the top end, which is expected in the turbulent flows. Here we can conclude that the turbulent flow in the channel becomes fully developed as it reaches the center of the channel, however as the flow proceeds further towards the outlet the full developed nature of the flow will be lost because of the geometrical constraints of the cooling channel which is circular in shape. Because of this reason, the non-dimensionalized mean velocity in the channel is plotted at the center of the channel because in that region the flow is fully developed.

Figure 4.13 illustrates the variation of u^+ plotted against y^+ for different Reynolds number as shown. The data obtained from the numerical simulation is plotted against the published results of Moser et al. [32] and Coles [10] and a good comparison is obtained except for the laminar sublayer region where the results from the present calculations deviate slightly with that of the published literature. The explanation of this minor mismatch maybe due to the shape of the cooling channel which is simplified into the rectangular channel flow. The values of constants used in the expression of log-law layer are $\kappa = 0.41$ and $C = 5.0$.

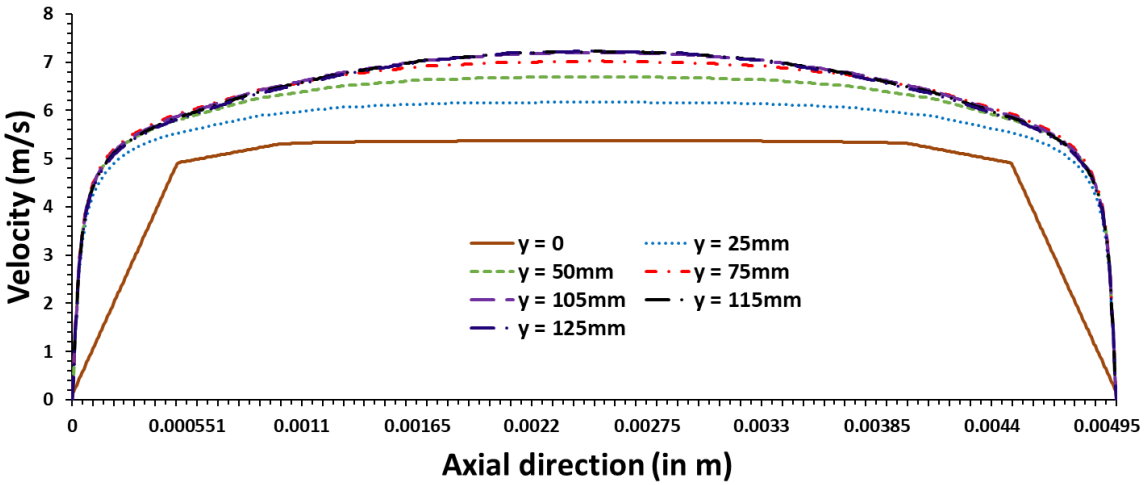

Figure 4.12: ***Velocity profile in the channel along the axial direction at different Y location for the inlet velocity of*** $4.58m/s$

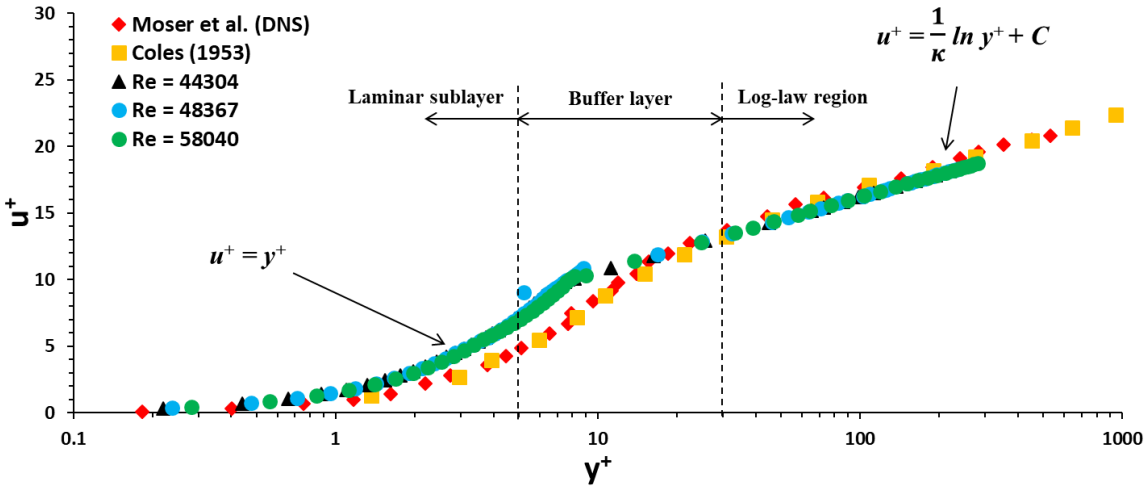

Figure 4.13: ***Comparison of non-dimensionalized mean velocity profile for fully developed turbulent flow between the results of Moser et al. [32], Coles [10] and the present simulation for three Reynolds numbers viz. 44304, 48367 and 58040***

The pressure drop in the cooling channel was calculated for various *Reynoldsnumbers* using Darcy Weisbach equation 4.1 and was compared with the corresponding values of pressure drop obtained numerically which is given in table 4.2. Figure 4.14 illustrates the variation of friction factor in the cooling channels for different *Reynolds numbers* for the present case which was calculated using the following relationship:

$$f = \frac{8\tau_w}{\rho \bar{u}^2} \tag{4.5}$$

where τ_w is the wall shear stress and the other symbols have their usual meaning. The values of friction factor obtained using equation 4.5 for different *Reynolds numbers* were plotted against the analytical (Blasius 2.16 and Petukhov 2.15 relationship) and the experimental data (Allen et al. [18]). From the figure 4.14, it can be concluded that a good match has been obtained and a minor mismatch may be attributed to the geometrical irregularity of the present case because the other data was plotted for channel flow.

Table 4.2: ***Comparison between the pressure drop in the cooling channel obtained numerically and analytically***

v_i	Re	Pressure drop (Analytical)	Pressure drop (Numerical)	% error
4.58	41022.74	7376.2511	7641.07	3.46
5	44784.65	8597.1656	8978.6	4.24
6	53741.58	11872.222	12623.32	5.95
7	62698.5	15677.778	16958	7.54
8	71655.43	20040.889	21866	8.34
9	80612.36	24941.111	27305	8.65
10	89569.29	30372.778	33294	8.77

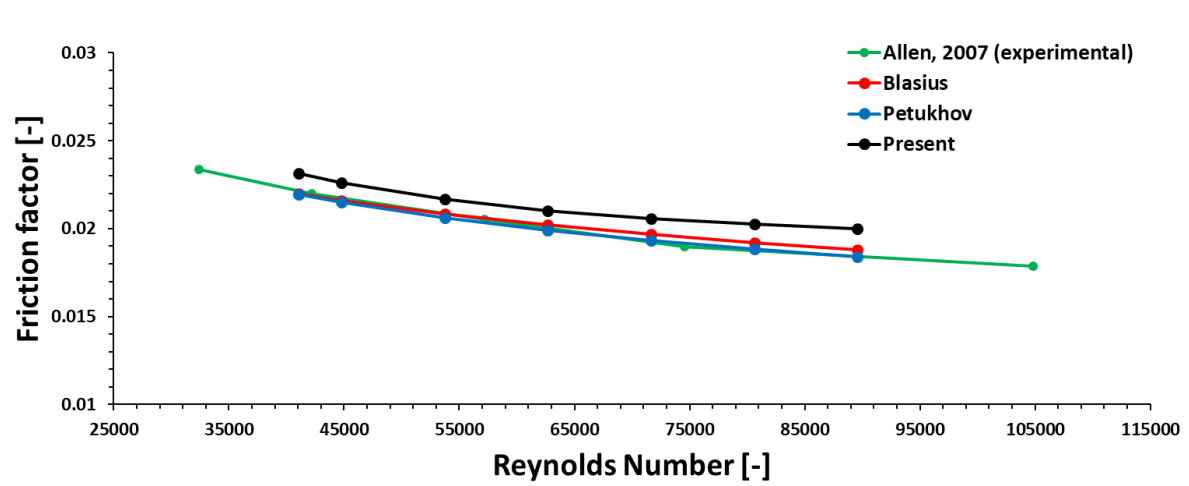

Figure 4.14: ***Comparison of friction factor in the cooling channel for the present case, analytical calculations and the experimntal data***

4.2. 3D full scale analysis

Section 4.1 concludes that the validations carried out for all the 2D and 3D cases shows good comparison with the analytical, numerical and experimental results and hence the full scale 3D model can be simulated now. Schematic diagram of the full scale 3D flow assembly along with the target blocks is shown in figure 2.1. As par the design parameter, the velocity of $5m/s$ should be maintained in the cooling channels and hence the velocity of $4.58m/s$ is given as the inlet boundary condition. $k\omega$ SST turbulence model is used for all the simulations in this section unless mentioned explicitly.

4.2.1. Computational mesh

Figure 4.15 illustrates the mesh for the present model which is hybrid in nature, consisting of both structured and unstructured elements. Non-conformal mesh was used at the interface of target and the cooling circuit. This was done because a grid with high mesh density is needed in the flow region as compared to the target domain and giving a conformal mesh at the interface would have unnecessarily increased the overall mesh size. In all the target blocks and the cooling channels, hexahedral elements are used which is imperative to improve the mesh quality (skewness, orthogonal quality etc.) leading to the faster convergence of the simulation. Wedge elements are being used in all the inflation layers near the wall region which basically forms the part of the boundary layer region. The inflation layers are necessary in turbulent flow simulations near the wall region in order to resolve the flow in the boundary layer region. Since the primary focus of this study is to resolve the flow in the cooling channels therefore with an aim to optimize the overall mesh, different inflation layers are given in the channels and manifolds region which is described as below:

- **Channel region:** The non-dimensional wall distance, y^+=1 is given in the cooling channels with 12 inflation layers (as shown in figure 4.16b) and a growth rate of 1.4.
- **Manifold region:** The velocity of water in manifolds is 5 times lower than that of channels, therefore y^+ >30 is used in this region with 6 inflation layers and a growth rate of 1.1.

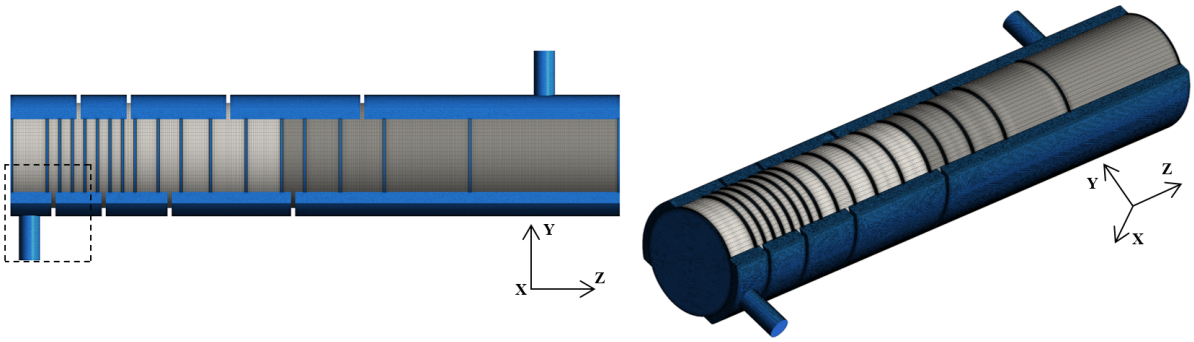

Figure 4.15: ***Computational hybrid grid used for the 3D simulations***

This process of giving different inflation layers in the cooling channels and in the manifold, reduced the total number of elements in the mesh by half of it's original size. In addition to the inflation layers, 8 elements were given in the axial direction and hence the cooling channels have 32 elements through it's thickness. Tetrahedral elements of size 2.5mm were given in all other parts of the cooling domain like manifolds, inlet pipe and outlet pipe (except channels). In the Ta2.5W cladding of 1.5mm width, 3 elements of size 0.5mm were given through its thickness. Because of the complexity of the computational domain, non-uniform heat deposition on the target blocks and highly turbulent nature of the flow in the cooling channels, the final mesh, as shown in figure 4.15 is very dense. Figure 4.16a shows the zoomed mesh of the part represented by the dashed rectangular marker in the above figure. The overall elements in the final mesh is around 19 million. A mesh sensitivity analysis was done for this model which is given in appendix A.

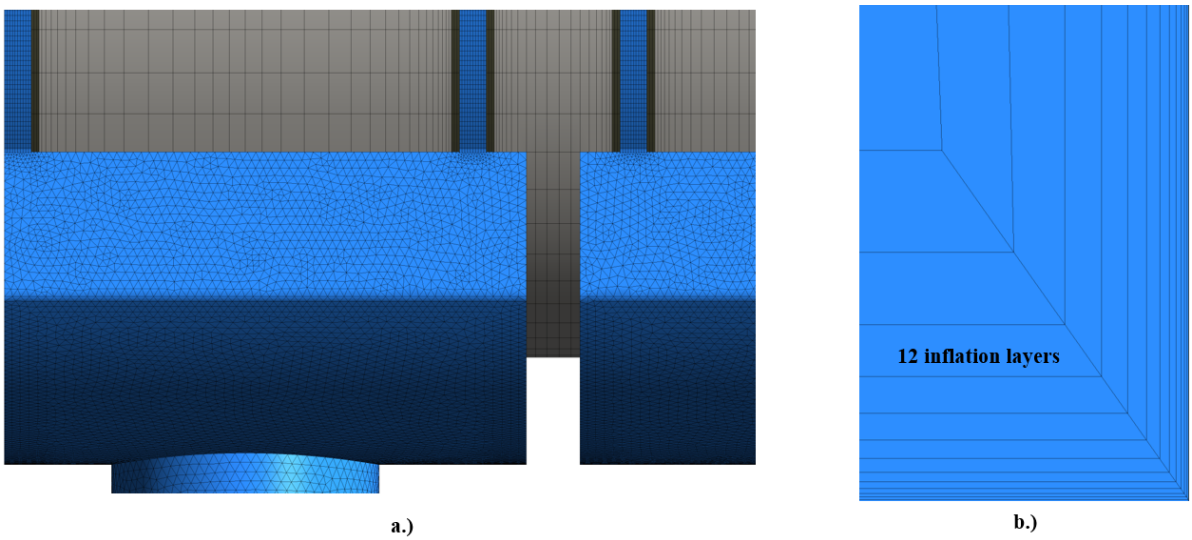

Figure 4.16: ***Zoomed part of the computational grid a.) of figure 4.15 (rectangular dashed box) b.) near the solid-liquid interface in the cooling channels***

Special attention was given while setting mesh parameters in the cooling channels because of its smaller size (5mm thickness). In addition to that it was observed that the mesh near the inlets and outlets of cooling channels usually collapses (specially in the inflation layer region of manifold) causing numerical fluctuations in the simulations finally leading to divergence, as all the channels merge into manifolds which are 4 times thicker. To avoid this problem, mesh optimization was done to obtained a better quality mesh which is illustrated in figure 4.17.

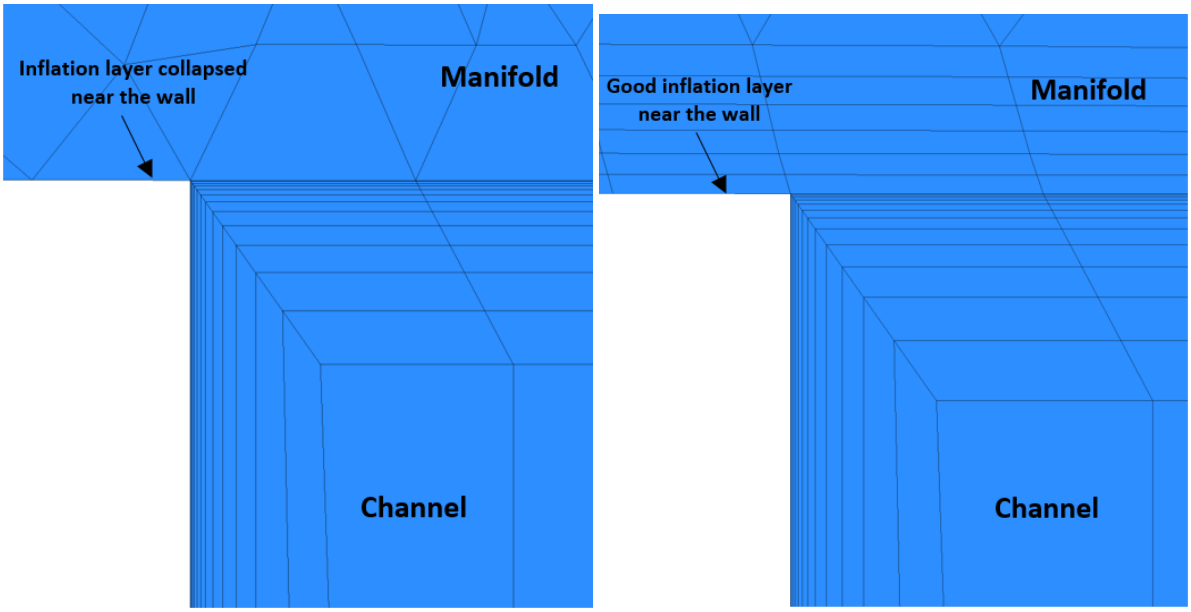

(a) poor quality inflation layer in manifold **(b)** good quality inflation layer in manifold

Figure 4.17: ***Comparison of mesh quality in manifold***

4.2.2. Steady state results

Figure 4.18 shows the contour for the static pressure distribution in the cooling system. As is illustrated in the figure, the pressure drop in the domain from inlet to the outlet is ~ 3.2 bar which means that the absolute pressure at outlet would be (20-3.2) bar =16.8 bar which is acceptable because the boiling temperature at this pressure is ~ $204°C$.

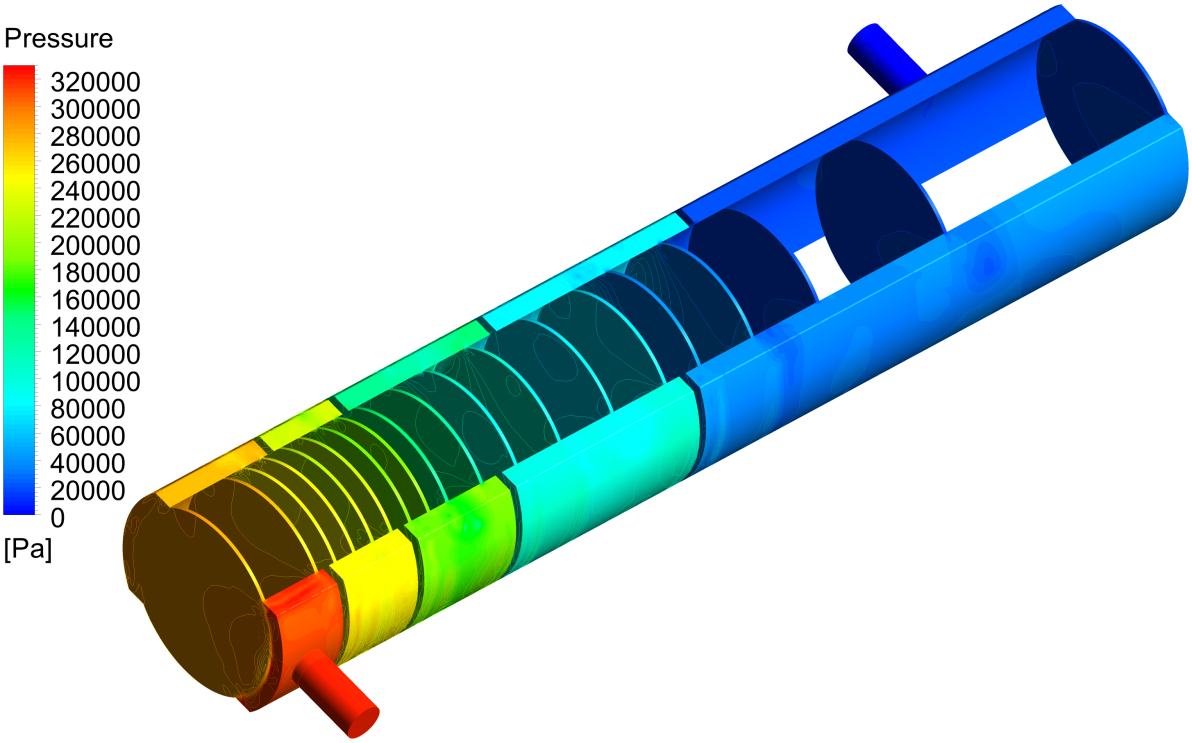

Figure 4.18: ***Pressure distribution inside the cooling system***

Figure 4.19 illustrates the velocity contour in the cooling domain along the YZ plane.

It is evident from this contour plot that the average velocity in all the cooling channels is approximately between 4 to 6m/s except for the last three channels where the average velocity is around 3 to 4m/s because of the reason given in section 2.1. In the manifolds and in the outlet pipe, the blue region denotes the re-circulation zones (because of flow separation) which is also visible in the 2D streamline plot shown in figure 4.20.

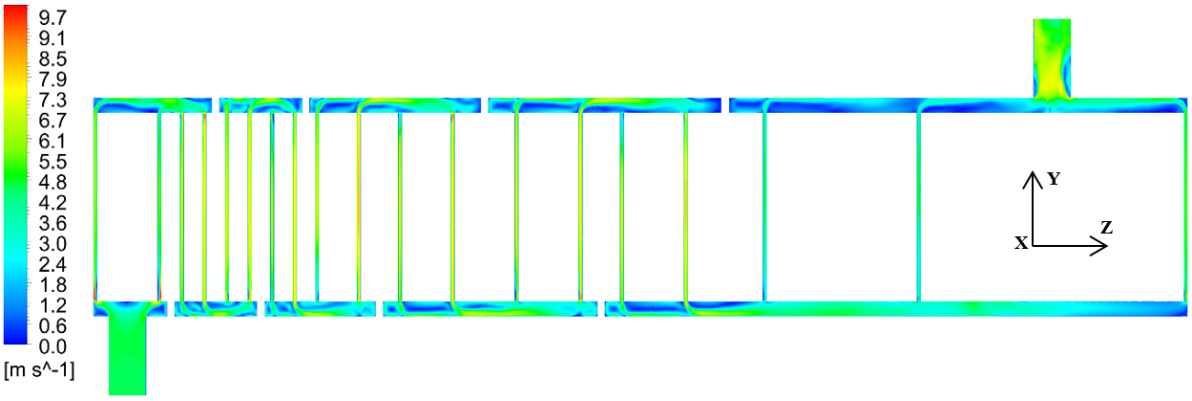

Figure 4.19: ***Velocity contour in the cooling system in YZ plane***

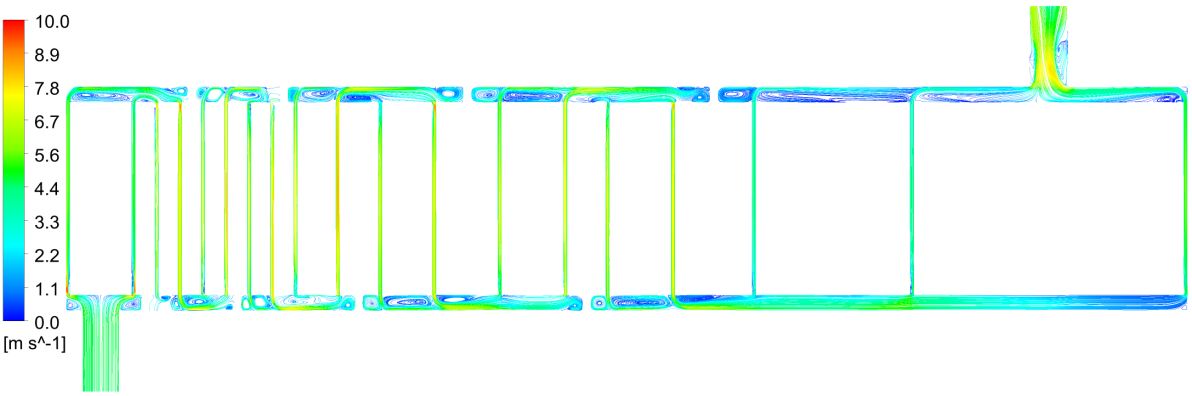

Figure 4.20: ***2D streamlines plot in the YZ plane***

The recirculation zone was also observed in the cooling channels because of their circular shape. Figure 4.21 illustrates the 3D velocity distribution in the cooling system with blue region in the channels showing the flow separation. The light green region at the inlet represents the uniform inlet velocity of 4.58m/s. The flow separation can be minimized (which will lead to comparatively smoother flow, uniform cooling and less pressure) by performing the shape optimization on the cooling domain which is beyond the scope of this thesis.

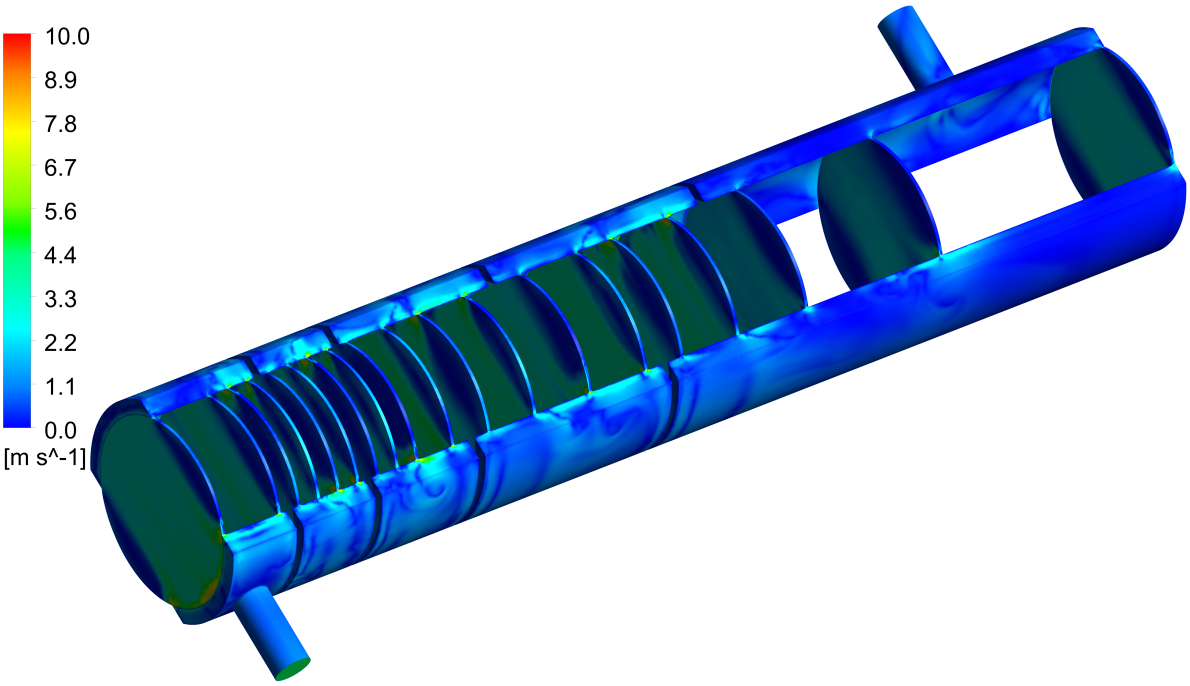

Figure 4.21: ***Velocity distribution in the cooling system with blue region in the channel showing the re-circulation zones.***

Figure 4.22 shows the plot for the average velocity of water in all the 19 channels. As can be seen from the figure, the average velocity in the channel is $\sim 5m/s$ for the first 16 channels and $\sim 3m/s$ for the last 3 channels. As water enters the cooling system from the inlet, it gets bifurcated into two streams which enter the channel with similar mass flow rate and hence the average velocity in the first two cooling channels is almost identical. However, due to the presence of blockers (which makes the serpentine design possible), the average velocity in every even channel is higher than that of the odd channels because of more mass flow rate entering the even channels. This is evident from figure 4.22 with the zig-zag pattern from channel 3 to 16. Thereafter, comparatively more mass flow rate enters the last channel and hence the average velocity in 19^{th} channel is higher than that of channel 17 and 18.

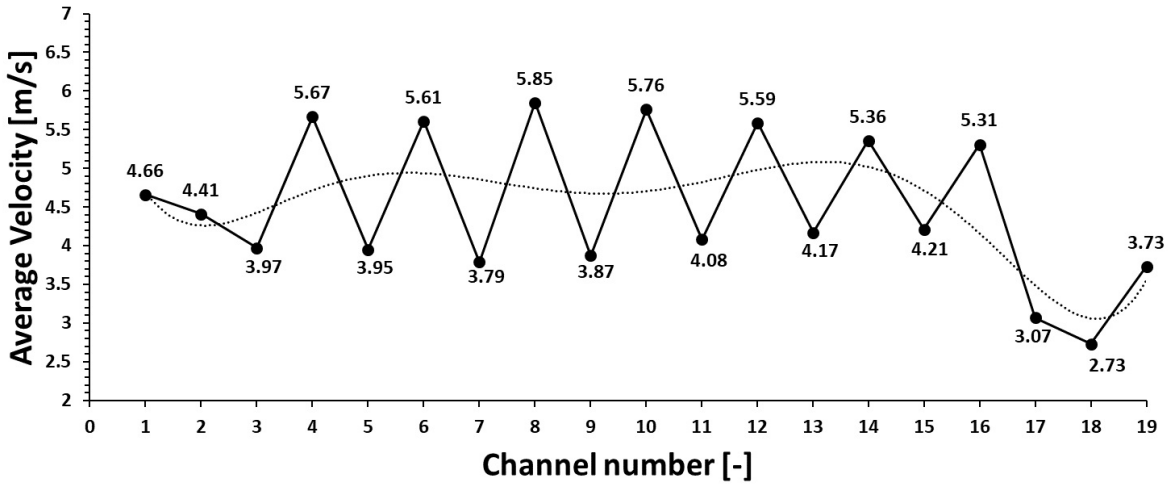

Figure 4.22: ***Variation of average velocities in the channels with · · · pattern as the trend-line.***

Figure 4.23 shows the y^+ distribution plot near the walls of the channels. From the figure,

we can see that the value of y^+ in all the walls of the channels is near 1 and hence we can conclude that the boundary layer is sufficiently resolved in the cooling channels using the $k-w$ SST turbulence model. The top and bottom red part has a y^+ value more than 30 because it is the part of the manifolds.

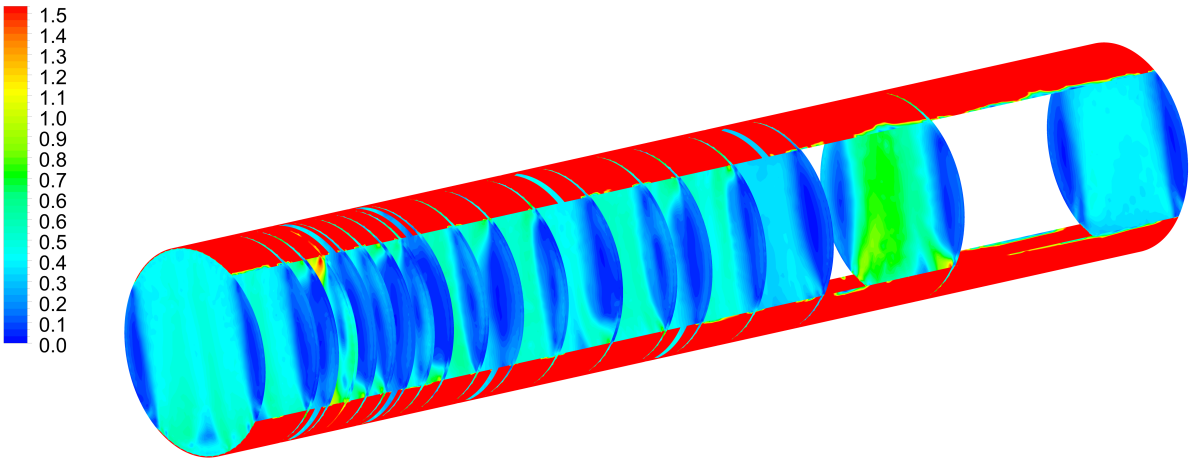

Figure 4.23: y^+ ***contour on the cooling channels***

As explained previously, due to the impact of the proton beam on the target, the total power deposited on all the blocks is $305kW$ as a result of which, the average outlet temperature of the cooling system was obtained around $34.8°C$. As the inlet temperature is $27°C$ therefore the total temperature rise at the outlet from the simulation is around $8°C$ which is found to be in good comparison with the temperature rise calculated from the energy balance (2.3). This behavior is illustrated in figure 4.24 which shows the temperature contour in the cooling circuit along the YZ plane. However in the transient case the temperature at the outlet will fluctuate depending on the beam impact with target in real time, which will be shown in section 4.2.3.

The temperature distribution in the core of all the targets is demonstrated in figure 4.25 which is a half section of the target blocks. As can be seen from the figure, the highest temperature reached in the target at steady-state condition is approximately $133°C$. Figure 4.26 shows the elucidated 2D temperature distribution along the YZ plane which is equivalent to the top surface contour of figure 4.25. As the shape of the proton beam impacting with the target blocks is in the form of circular ring (with thickness $16mm$ and at a mean radius of $50mm$ from the axis) and hence it is expected to see in the 2D section a temperature contour with 2 hot spots (maximum temperature) on each target, at a distance of $50mm$ from the axis of the target as can be seen in figure 4.26. The maximum temperature is found to be in block 12 which is expected because it has the maximum power deposition as well (figure 1.4). The temperature contour in the last three blocks is spatially more diffused as compared to other blocks, because of their large thickness (100, 200 and 350 mm) and relatively lower power deposition.

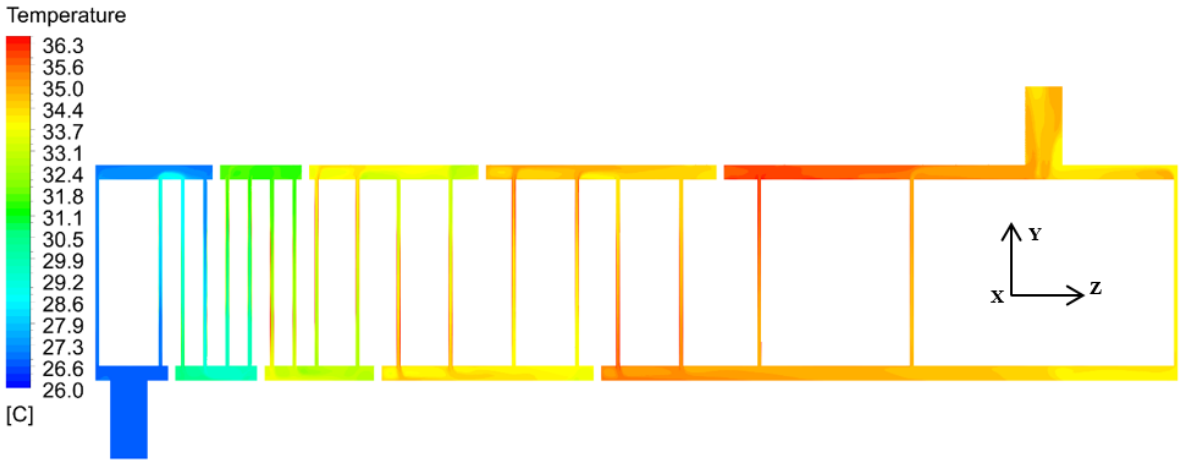

Figure 4.24: ***Temperature contour in the cooling circuit along the YZ plane at steady state.***

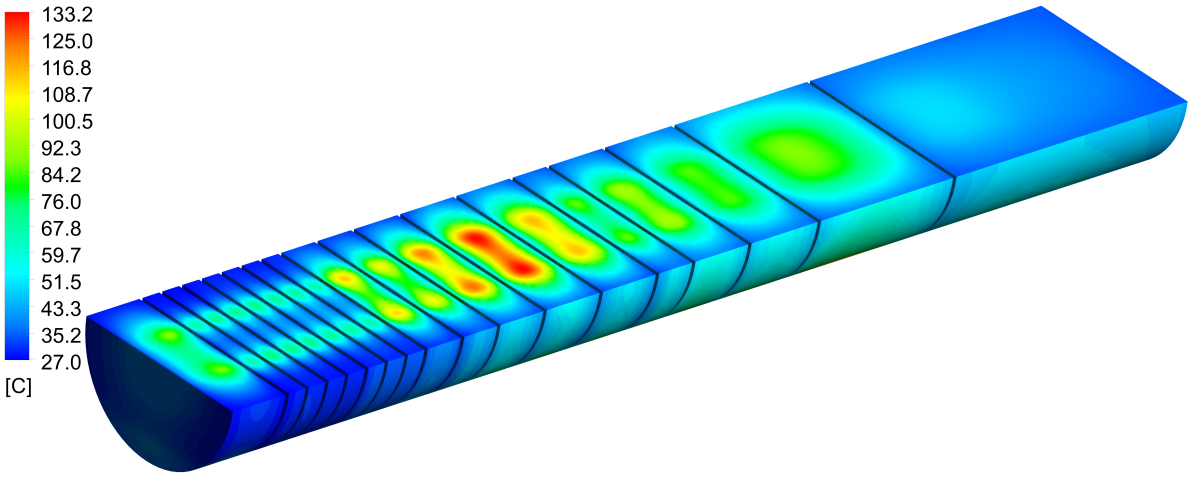

Figure 4.25: ***Temperature contour in the target blocks at steady state.***

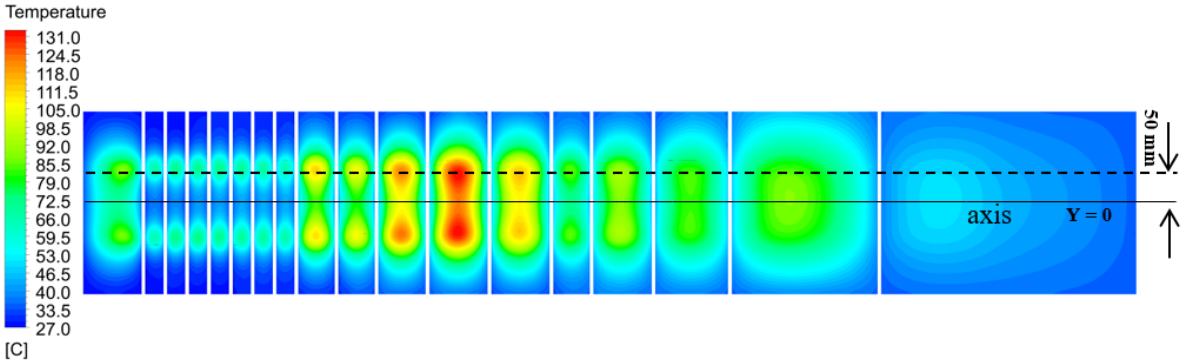

Figure 4.26: ***Temperature contour in all the blocks along the YZ plane***

Figure 4.27 shows the temperature distribution on the surfaces of the full assembly (4.27a) and on the outer surface of the blocks (4.27b) respectively. In figure 4.27b it can be observed that the part of the target (top surface), which is not in direct contact with the flowing water is comparatively hotter than the surface over which the water is flowing continuously through manifold (side surface). The maximum temperature in the target blocks as seen from figure

4.25 is ~ 133°C, however in this case the maximum temperature on the surface of the target is ~ 70°C and is obtained on target 17.

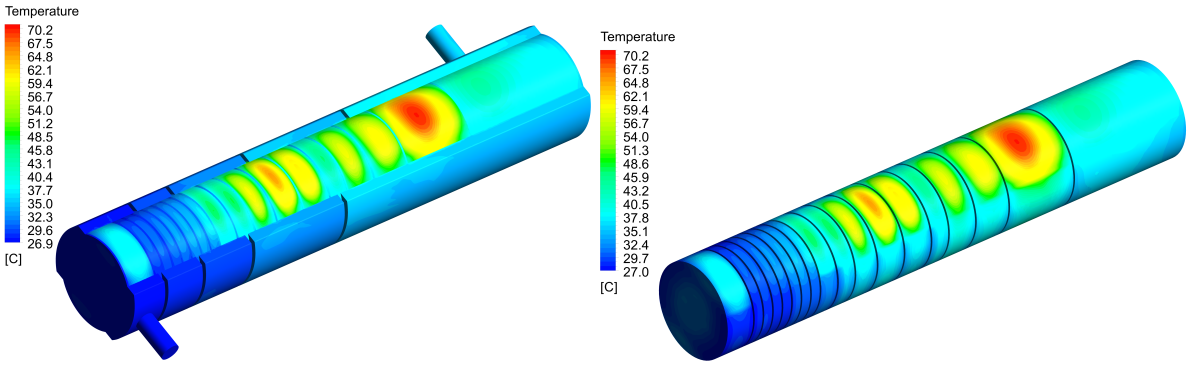

(a) Full assembly **(b)** Target blocks

Figure 4.27: ***Temperature contour in the target blocks and cooling domain at steady state***

Figure 4.28 shows a plot for temperature variation in all the blocks at a distance of 50mm from the axis of the target (as shown by dashed line in figure 4.26). All the 18 target blocks are represented by the individual temperature curves extending until 1.45m with the maximum temperature shown for every individual block on the top of the curves. From the plot it can be seen that the value of maximum temperature in block 12 is 128°C (however this is not the absolute maximum temperature of block 12, but the temperature obtained at the location, 50mm from the axis), however in the transient case, at peak of the pulse the maximum temperature reached inside the target blocks is higher, which is explained in section 4.2.3. Figure 4.29 shows the temperature contour in block 12 in 3D view and in a slice taken at the middle of the block in XY plane. Figure 4.29b shows that the temperature distribution on the target is non-uniform and is influenced by the water flowing in the serpentine way. It can again be confirmed independently from figure 4.29a (which was also shown in figure 4.27) that the region of target (top surface) not in direct contact with water has almost double temperature as compared to the region of target (side surface shown by blue contour) in direct contact with water through the manifold.

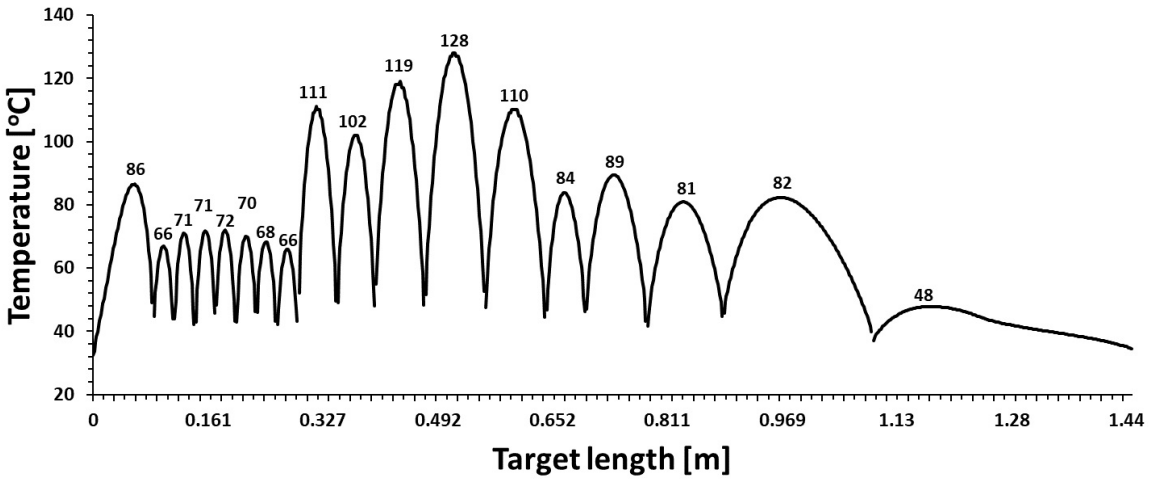

Figure 4.28: ***Temperature variation in all the target blocks at Y = 50mm***

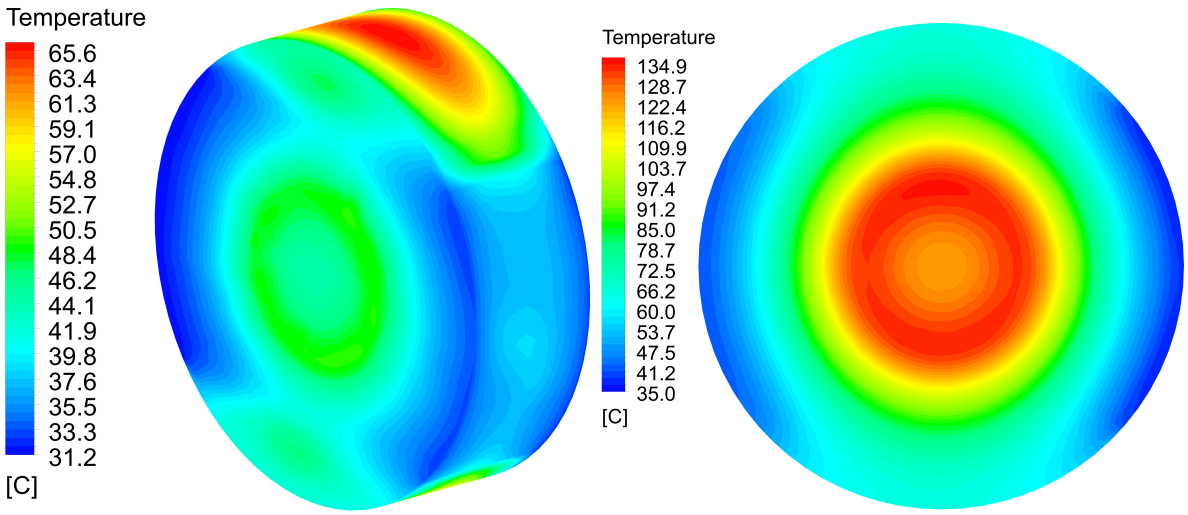

(a) 3D view **(b)** middle section

Figure 4.29: ***Temperature contour in*** 12^{th} ***block at steady state***

It can be concluded from figure 4.26 and 4.29 that the maximum temperature in the core of the blocks is not necessarily found at $50mm$ from the axis of the targets even though it is the mean position of the beam impact. This is primarily because of the two reasons: a.) heat conduction from the beam impact location towards the center of the target material in the steady state condition and b.) high velocity of water flowing in the channels which diffuses the energy from the blocks and hence make changes in the location of maximum temperature within the block. Therefore figure 4.28 doesn't show the absolute maximum temperature in the blocks, rather it must be calculated using a function to find the maximum value of temperature in block who's position can be variable for each block. Figure 4.30 shows such a plot where the maximum value of temperature for every block is illustrated from where we can observe that the actual maximum temperature in 12^{th} block is $135.8°C$.

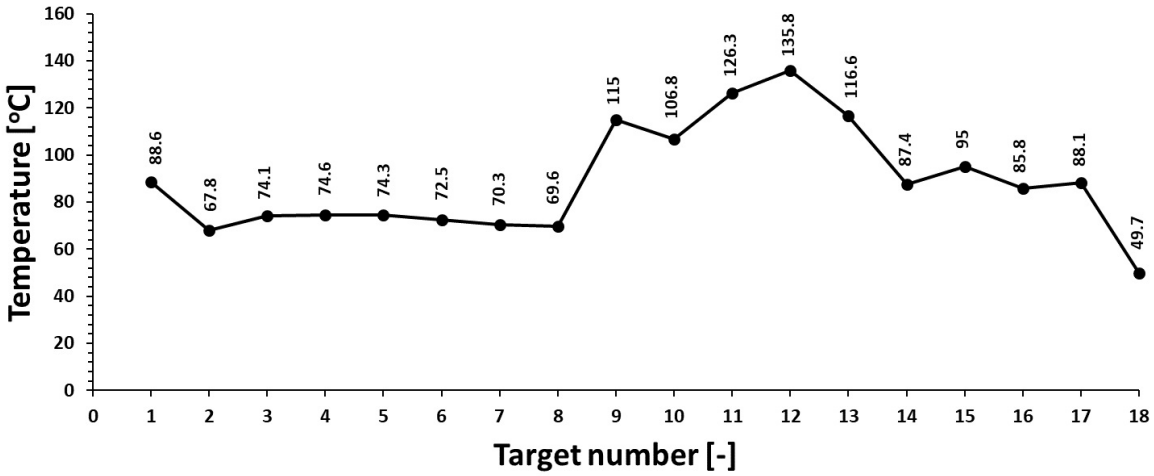

Figure 4.30: ***Maximum temperature at the core of all the target blocks***

Figure 4.31 shows the comparison of average surface temperature at the same location between analytical calculation (calculated in the similar way as shown in section 4.1.1) and numerical simulations for two turbulence models (kw SST and $k\epsilon$ EWT). Here it can be observed that the surface temperature obtained from $k\omega$ SST model is much closer to the analytical result in contrast with that obtained from $k\epsilon$ EWT model and hence it can be stated that the

latter model under-predicts the results as compared to the former turbulence model. Figure 4.32 shows the comparison of average heat transfer coefficient for all the 19 channels of the cooling domain between analytical values (calculated in the similar way as shown in section 4.1.1), kw SST and $k\epsilon$ EWT turbulence models. The analytical plot is obtained using the average channel velocities as shown in figure 4.22. From this plot as well we can conclude that the HTC values obtained using $k\omega$ SST turbulence model is in good comparison with analytical solution and hence $k\omega$ SST model must be used for such complex flow problems in order to get accurate results.

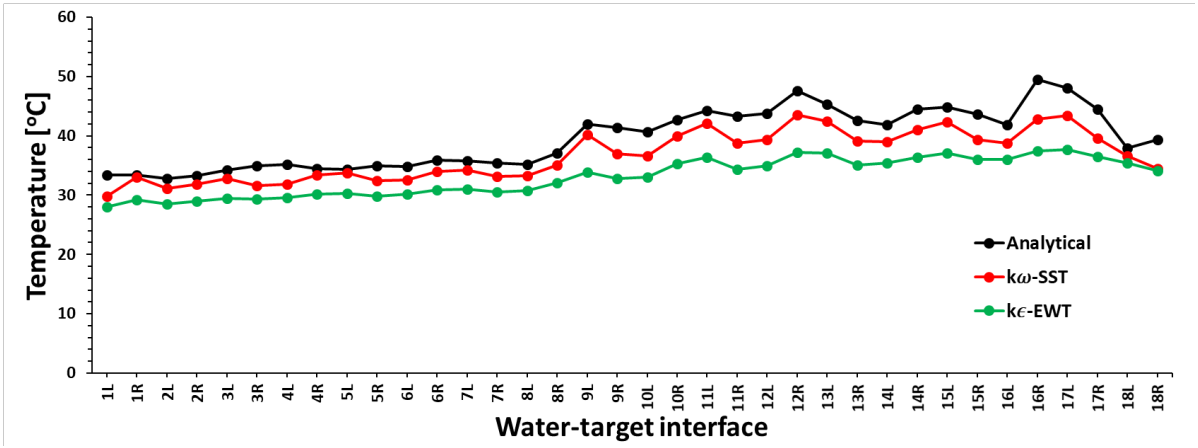

Figure 4.31: ***Comparison between average water-target interface temperature in the channels obtained from analytical calculations and numerical simulations ($k\epsilon$ EWT and $k\omega$ SST turbulence models).***

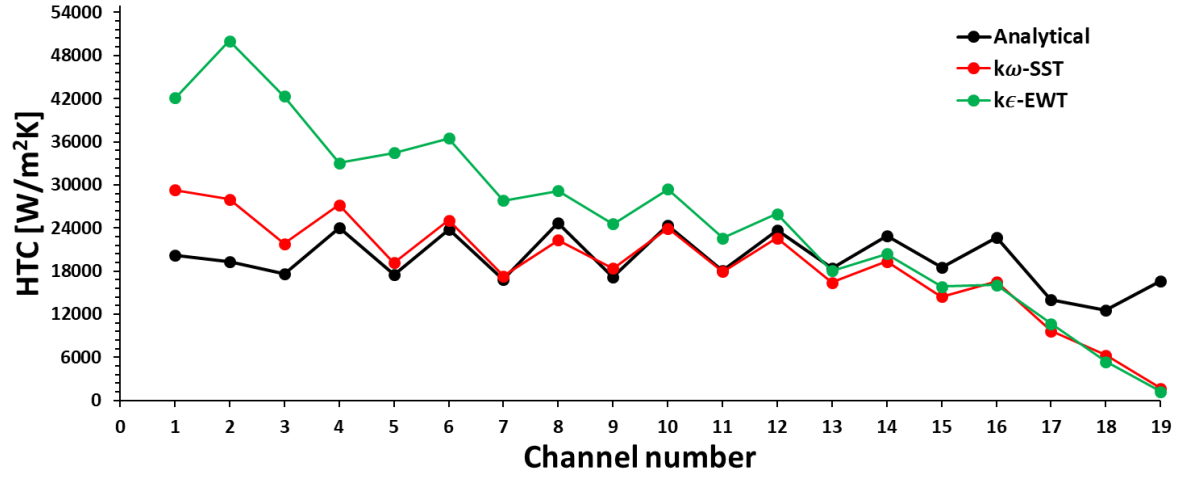

Figure 4.32: ***Comparison between average HTC in the cooling channels obtained from analytical calculations and numerical simulations ($k\epsilon$ EWT and $k\omega$ SST turbulence models).***

The HTC, as explained earlier, is dependent on the flow velocity and contact area of the interface and as a general rule of thumb the more flow velocity is, more is the value of HTC. A comparative study to investigate the effect of different channel velocities (1, 2.5, 5, 7.5 and 10 m/s) on the value of average HTC in the cooling channel was done as shown in figure 4.33. A good comparison was found between the average value of HTC obtained numerically and analytically (2.2). From this figure it is concluded that the heat transfer coefficient on the solid-liquid interface increases as the velocity of water is increased. However on the negative side, high velocities in the channel causes erosion/corrosion on the walls of the solid surface and higher pressure drop (Darcy Weisbach equation) therefore special care must be taken before assigning high velocities of water in the channels.

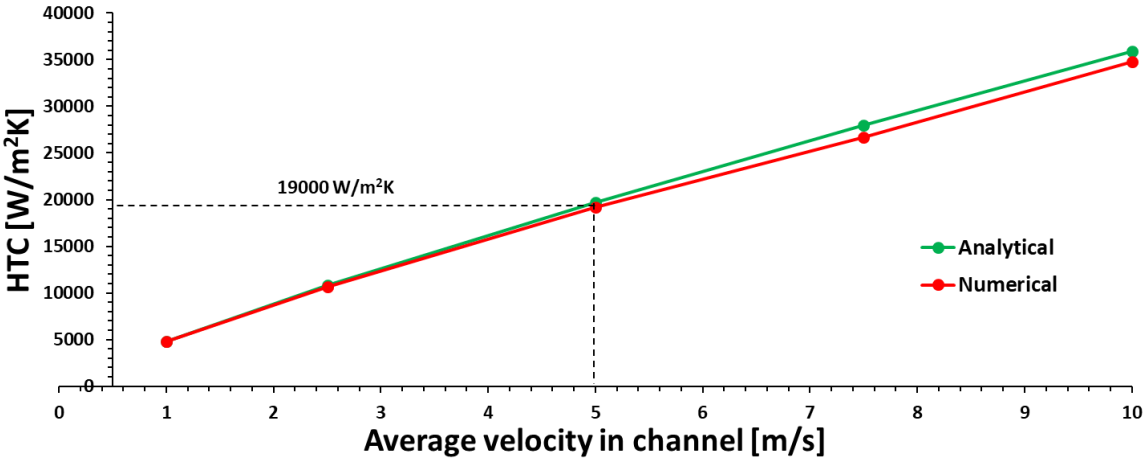

Figure 4.33: ***Variation of convective heat transfer coefficient with channel velocity***

Figure 4.34 illustrates the HTC distribution on the solid-liquid interface for 9^{th}, 10^{th}, 11^{th} and 12^{th} blocks where it can be seen that locally higher values of HTC are reached on the surface. For both interfaces of each block, it can be observed that for odd blocks the right interface has comparatively higher value of HTC and vice-versa for even blocks. This is attributed to the higher velocities in that particular channels as can be seen from figure 4.22.

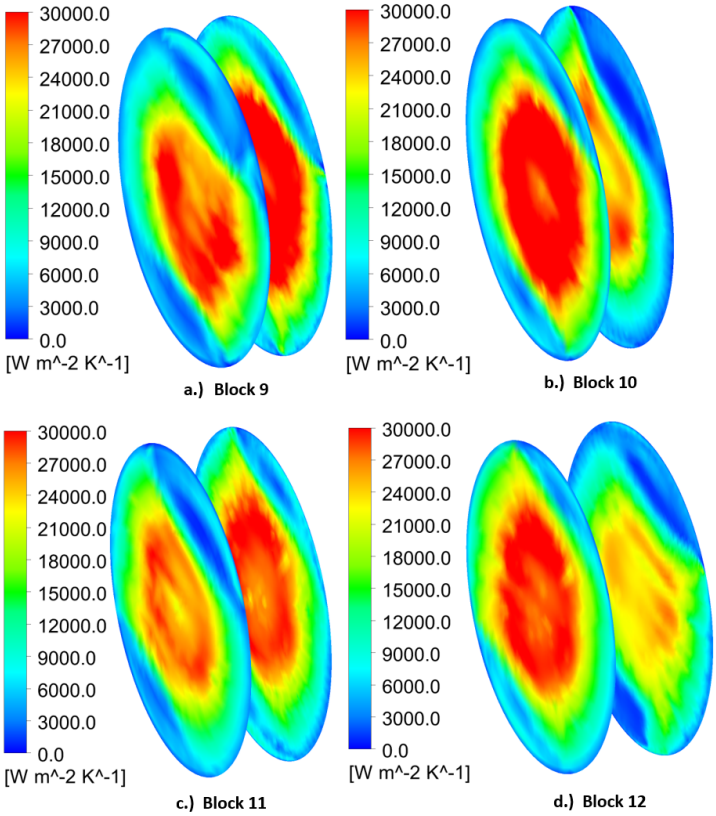

Figure 4.34: ***Convective heat transfer coefficient distribution on water-target interface of different blocks in the channel***

4.2.3. Transient results

Transient simulations were performed for the same model as described in the aforementioned section with identical beam size, computational grid and the boundary conditions. In this case, the UDF which imports the energy deposition map on the target blocks was modified such that the energy of 400 GeV SPS proton beam was imposed on all the targets for 1 second and then it was turned off for 6.2 seconds, thereby forming a cycle of 7.2 seconds (as shown in figure 1.2). Likewise 3 cycles were simulated which comprises of the total physical time of 21.6 seconds. The transient simulations were carried out by providing the results of steady simulations as the initial condition. Time step size of 0.05 second was used and a total of 432 number of time steps were simulated which comprises of 21.6 seconds of the physical time. These simulations were performed on a HPC cluster of CERN with 64 physical cores and 512GB RAM and it took 4.5 days to converge the full solution.

Figure 4.35 illustrates the temperature distribution contour in all the target blocks at a slice taken along the diameter at the peak of the pulse (1 second). The corresponding temperature profile at a distance of 50mm from the axis is plotted in figure 4.36. From this figure, it can be noticed that both block 9 and 12 have similar maximum temperature in the core of the target (however, as explained for figure 4.28, this plot doesn't illustrate the absolute maximum temperature inside the core of the target blocks). In contrast with figure 4.28, here the maximum temperature in blocks 2 to 8 is approximately double because this plot is obtained at the peak of the pulse and the energy density is higher in this blocks as shown in Figure 1.5.

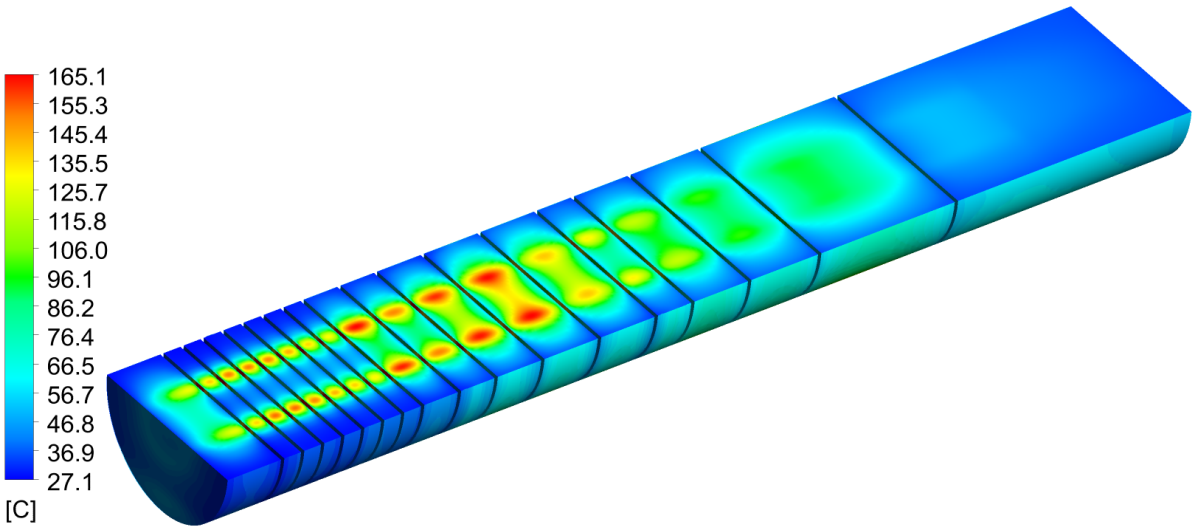

Figure 4.35: ***Temperature contour in the target blocks at the peak of the pulse (1 second)***

Figure 4.37 shows the temperature distribution in block 12 at the peak of the pulse and in contrast with figure 4.29b, the maximum temperature in the core of the block 12 is 165°C (figure 4.37b), which is around 30°C higher than that in steady case. It can be again observed from figure 4.37a that the section of the block (top and bottom surface) which is not in direct contact with the water is nearly 30°C more hot than the side surfaces which is cooled by the water through the manifold.

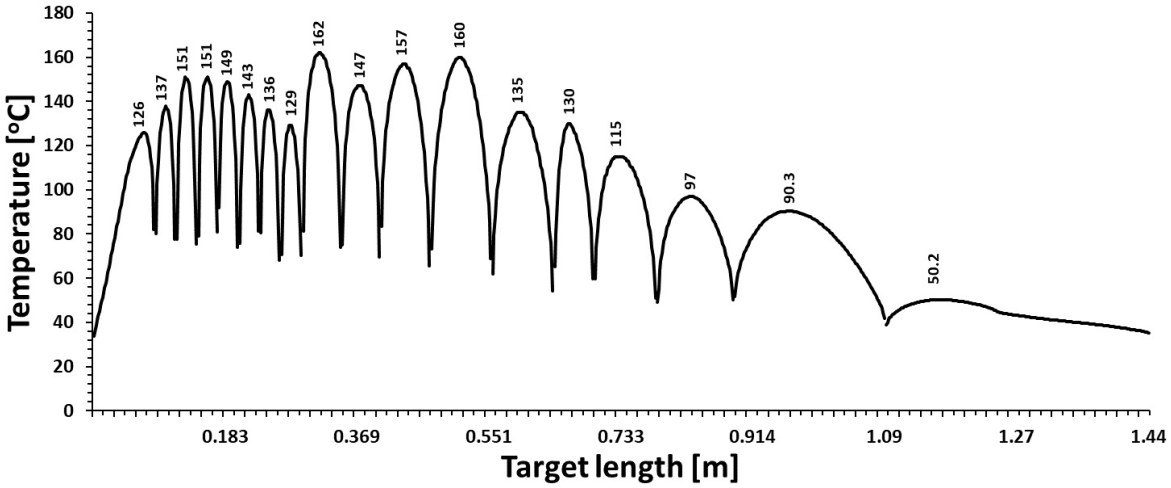

Figure 4.36: ***Temperature variation in all the target blocks at the peak of the pulse at Y = 50mm***

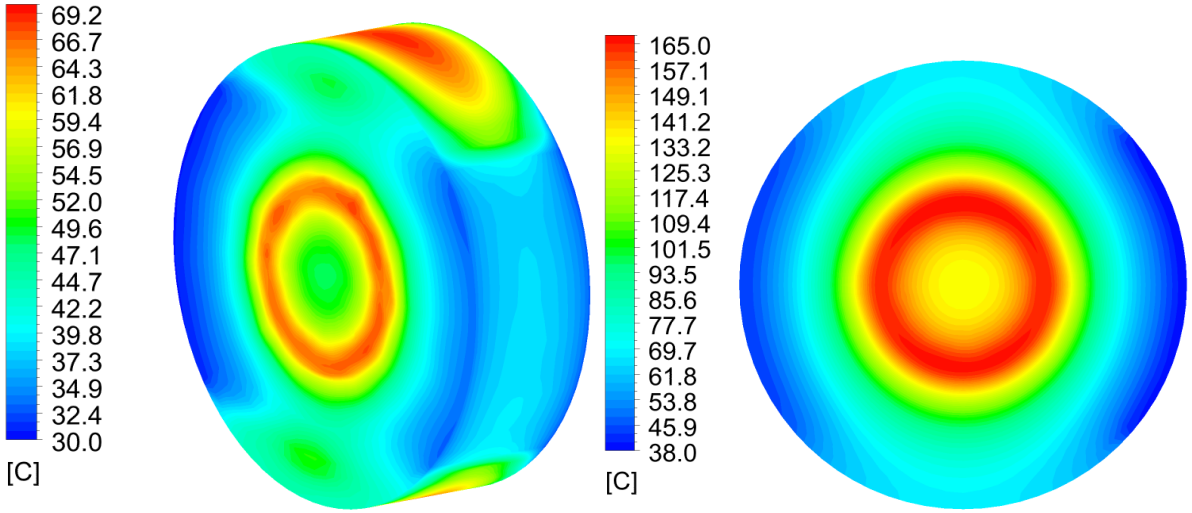

(a) 3D view **(b)** middle section

Figure 4.37: ***Temperature contour in 12^{th} block at the peak of the pulse (1 second)***

As explained earlier, each target block has a cladding of $1.5mm$ of Ta2.5W which is comparatively very thin as compared to the core of the blocks and hence it is important to investigate the maximum temperature reached in the Ta2.5W cladding in order to ensure that the mechanical failure doesn't occur due to excessive thermal stresses. Figure 4.38 and 4.39 shows the maximum temperature inside the core of target blocks and Ta2.5W coating at the peak of the pulse. Figure 4.38 shows that the maximum temperature in target is found to be in block 12 is $166.4°C$, however the maximum temperature in block 9 which is $165.5°C$ is quite close to the value of block 12. As there are 18 target blocks and hence there are 36 Ta2.5W coating (on both circular faces of targets) and the maximum temperature inside these coatings at the peak of the pulse is illustrated in figure 4.39 which is obtained in the left side coating of block 3 and 5 whose values are $119.7°C$ and $120.3°C$ respectively.

Figure 4.40 shows the maximum temperature on the surface of the target blocks and it can be seen that the surface having highest maximum temperature is the left surface of target 3 and 5 and it's value is $89.8°C$ and $89.3°C$ respectively which is more than 2 times lower than the boiling temperature of water at $20bar$. From here it can be concluded that during normal operation, the convective heat transfer will take place smoothly even at the peak of the pulse.

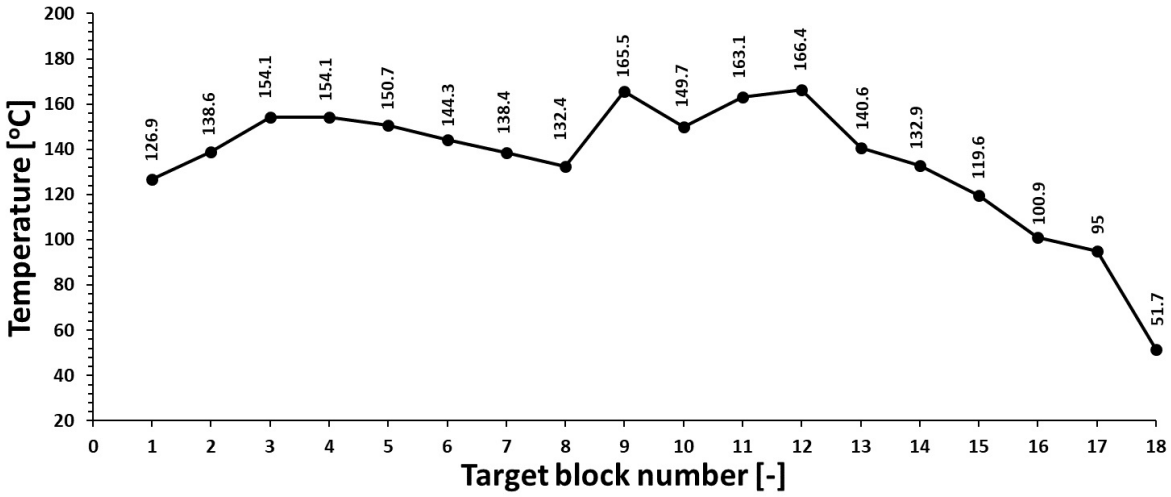

Figure 4.38: ***Maximum temperature in the core of target blocks at the peak of the pulse***

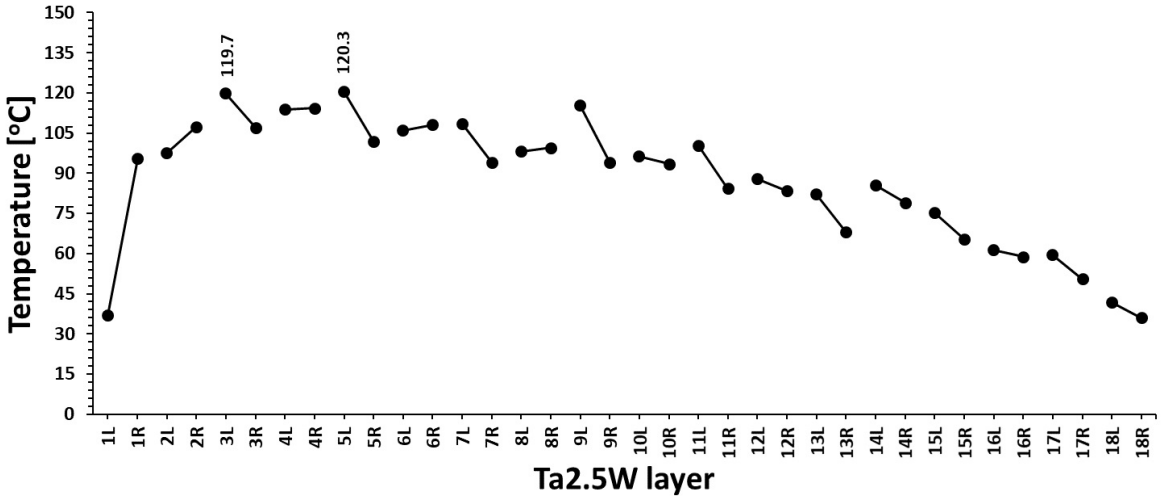

Figure 4.39: ***Maximum temperature in the Ta2.5W coating at the peak of the pulse,***

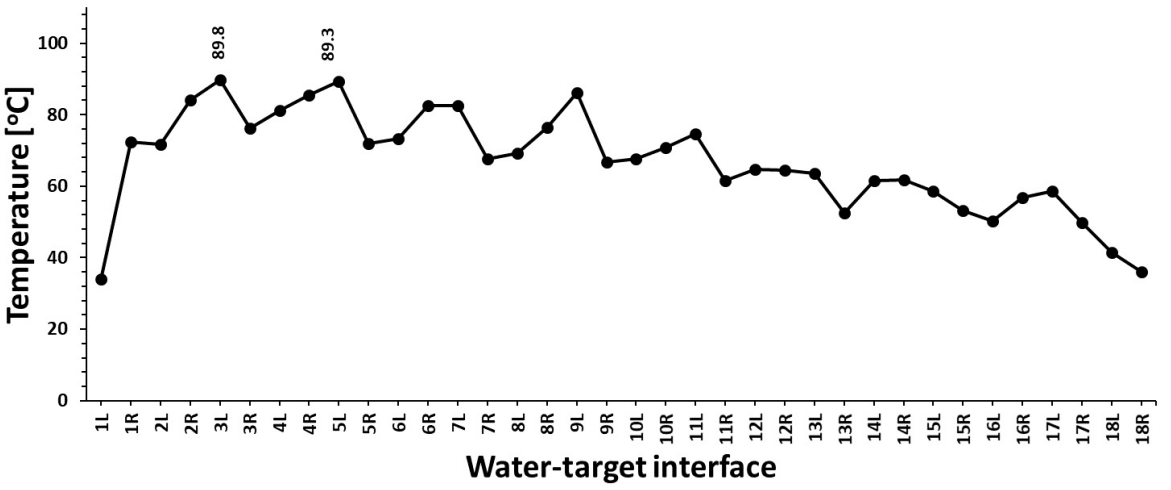

Figure 4.40: ***Maximum surface temperature on the target blocks in the channels at peak of the pulse.***

Figure 4.41 shows the evolution of maximum temperature in TZM (9 and 12) and W blocks (14) blocks with time. This plot illustrates the thermal response of target blocks during pulse period (1 second) and cool-down period (6.2 seconds). Also from figure 1.4 we had seen that the total power deposition on block 12 is slightly greater than that in block 9 and hence figure 4.41 shows a slightly higher temperature for block 12 at the peak of the pulse. As can be observed from this figure, during cool-down period blocks 9 and 14 dissipates more energy as compared to block 12 because the latter is wider as compared to the other 2 blocks.

The temperature contour in the target blocks at a slice taken in YZ plane at different time is shown in figure 4.42. The spill or the pulse duration (0 to 1 second) is shown from figure 4.42a to 4.42f and figure 4.42g illustrates the temperature contour inside the 2D section of target blocks at the end of the cool down period, that is 7.2 seconds. As can be seen from the color bands of this figure, the temperature inside the target increases until the peak of the pulse and then it drops to a lower value at the end of the cool-down period, which is also elucidated in figure 4.41. In contrast with the temperature contour seen in the steady state case (figure 4.26), here the temperature distribution plot is less diffused towards the center of the target as can be seen from the figure 4.42f which is the peak of the pulse.

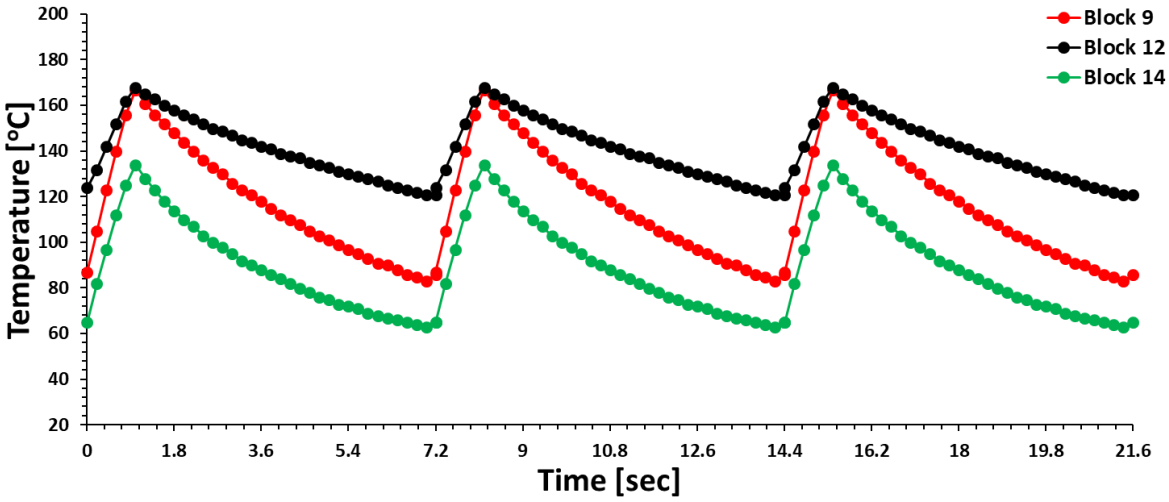

Figure 4.41: ***Comparison of maximum temperature distribution in time for TZM (9 and 12) and W (14) target blocks.***

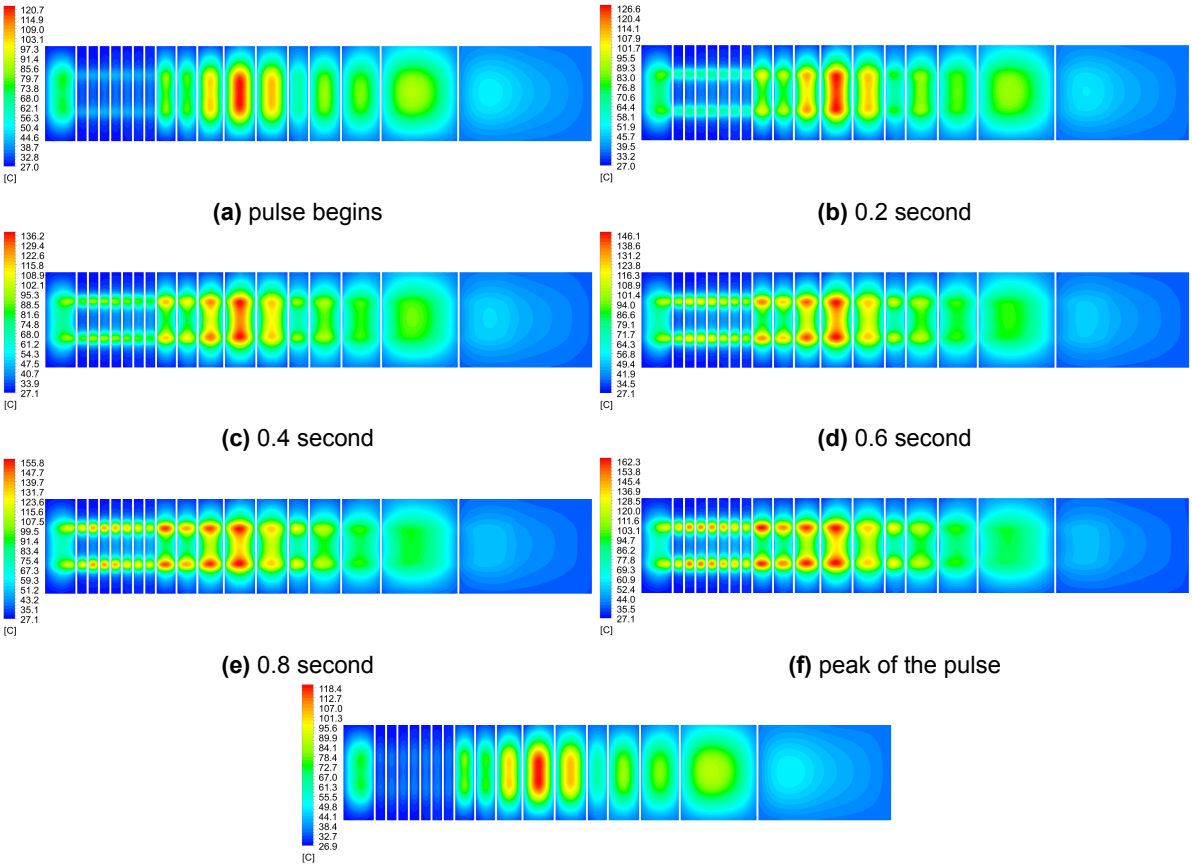

(a) pulse begins

(b) 0.2 second

(c) 0.4 second

(d) 0.6 second

(e) 0.8 second

(f) peak of the pulse

(g) end of the cool-down period

Figure 4.42: ***Temperature contour in all the target blocks along the YZ plane at different time***

5

Conclusion

The Beam Dump Facility (BDF) target is a new facility which is foreseen to be installed in the North Area of the CERN. The design and optimization of the cooling system of this facility is one of the most difficult aspects because of its geometrical complexity. A three dimensional numerical model to simulate the conjugate heat transfer in the cooling system of the Beam Dump Facility (BDF) target is developed using the commercial CFD code *ANSYS Fluent* [1] where water is used as the coolant . The total power deposited on all the 18 target blocks is $305kW$ and to dissipate that, a serpentine design of the cooling system with two parallel uni-directional channels was finalized having 19 channels in total on both sides of the target blocks. The design value of water velocity in the cooling channels of thickness $5mm$ is $5m/s$ and the system pressure is maintained at $20bar$.

The average Reynolds number in the channels is around 48000 which makes the flow highly turbulent in nature. Hence, the $k-\omega$ SST [24] turbulence model was used to simulate the flow behaviour in the cooling system because of its ability to resolve the flow in the laminar-sublayer near the wall and in the core region. It was observed that for the similar mesh size $k-\omega$ SST model gives better results as compared to $k-\epsilon$ enhanced wall treatment (EWT) model and hence the former model was used for the rest of the study.

Due to the complexity of the cooling system, it was very challenging to validate the full scale results with analytical or published results therefore a 2D section of the full scale assembly was simulated for this purpose. The pressure drop in all the 19 channels was found in accordance with the analytical calculations using Darcy Weisbach equation. The *Biot number* for all the target was found to be much greater than 1 and hence the lumped capacitance model can't be used for this numerical model. The temperature profile in the target blocks for the 2D case, obtained numerically was plotted against the one dimensional conduction equation with heat generation and a good comparison was achieved for all the target blocks where height to thickness ratio of the blocks is $\gg 1$. However, for the last two blocks where the height to thickness ratio is equal to or less than 1, a mismatch between the analytical and numerical results was seen because of the violation of 1D approximation of the numerical results.

Subsequently a three dimensional channel with the dimensions similar to the channels used in the actual assembly was simulated to validated the flow behaviour. From the streamlines and the velocity contours, it was concluded that the flow in the cooling channels can be simplified to the rectangular channel flow because of the presence of strong re-circulation zones on the circular end of the channel. It was also observed that the flow in the channel becomes fully-developed at the centre of the channel and beyond that point the full-developed nature of the flow starts to disappear because of the geometrical reasons. The non-dimentionalized mean velocity profile (u^+ vs y^+ plot) at different *Reynolds number* was plotted and a good match was obtained against the results of Moser et al. [32] and Coles [10]. Subsequently the friction factor for different Re obtained using the present model was plotted against the analytical calculations (Blasius and Petukhov relationships) and the experimental results of Allen et al. [18].

After performing these validation and verification cases, the full-scale 3D model of the cooling assembly along with the target blocks was simulated. A user defined function (UDF) was used to import the non-uniform energy map in the present model which was obtained via $Fluka$ MonteCarlo simulations. The pressure drop from inlet to the outlet of the cooling system was obtained around $3.2bar$ and the average velocity in the channels was achieved near $5m/s$, except for the last three channels because of comparatively less mass flow rate passing through them. Lots of re-circulation zones were observed in the cooling system, because of its complex geometry. Shape optimization can be performed on the cooling circuit to minimize the re-circulation zone which will facilitate better heat transfer with lower pressure drop, which is beyond the scope of this thesis. A temperature rise of around $8°C$ with the outlet temperature of $34.8°C$ was achieved which is in accordance with the heat conservation. As the energy deposition profile on the target blocks is in the shape of circular ring with the mean radius of $50mm$ from the axis of the target and hence the temperature distribution contour was found to be diffused towards the centre of the target blocks. The maximum temperature in the target is $128°C$ and $166.4°C$ for the steady and transient cases respectively, which was achieved at the 12^{th} block in both cases. The average HTC in different channels was plotted against the analytical calculations and a good comparison was obtained. Similar analysis was done for various average velocities in the channels and the results obtained were found in good accordance with the analytical calculations. The maximum target water interface temperature at the peak of the pulse (1 second) was found to be around $90°C$ on the surface of 3^{rd} block which is sufficiently below the boiling temperature of water at $20bar$. As a future work, this study can be extended by the implementation of large eddy simulation (LES) or direct numerical simulation (DNS) with more powerful computational facilities.

A Temperature dependent property data

As explained in section 1.3.1, the temperature dependent property data [35] for TZM and Tungsten blocks were used for the steady and the transient simulations as given below:

A.1. Property data for TZM

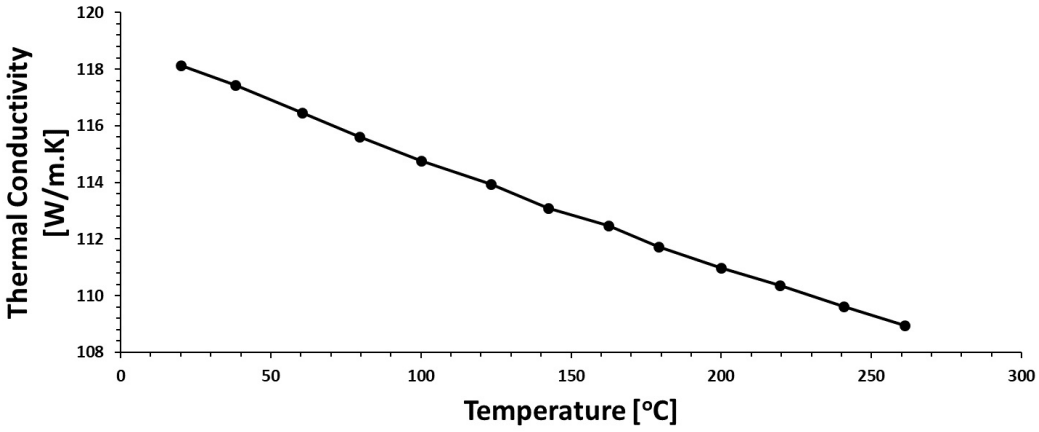

Figure A.1: ***Variation of thermal conductivity of TZM with temperature***

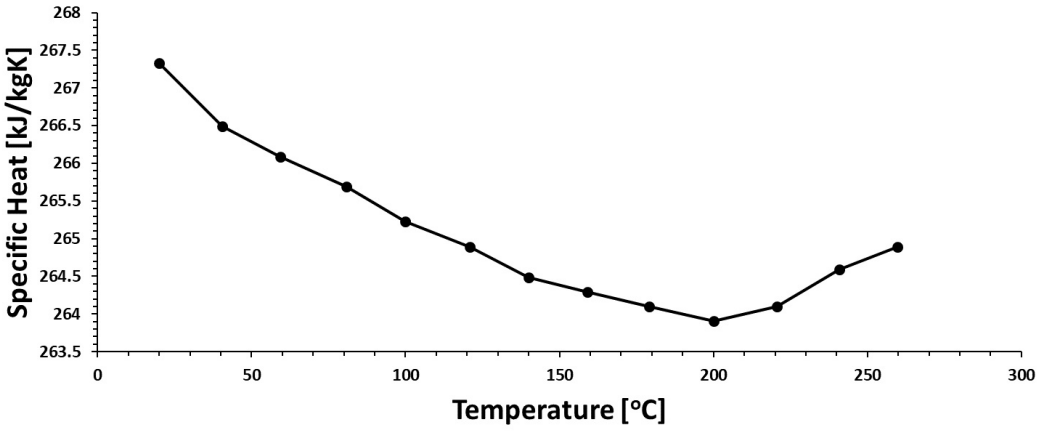

Figure A.2: ***Variation of specific heat of TZM with temperature***

A.2. Property data for Tungsten

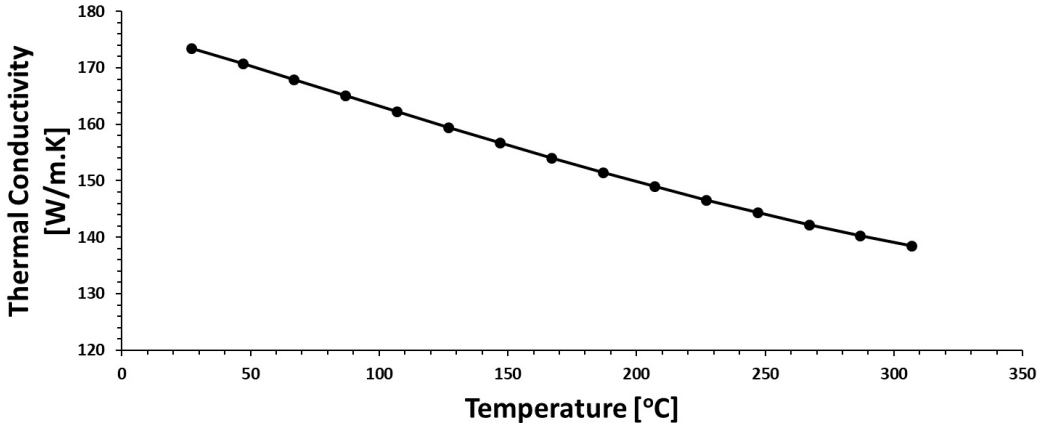

Figure A.3: ***Variation of thermal conductivity of Tungsten with temperature***

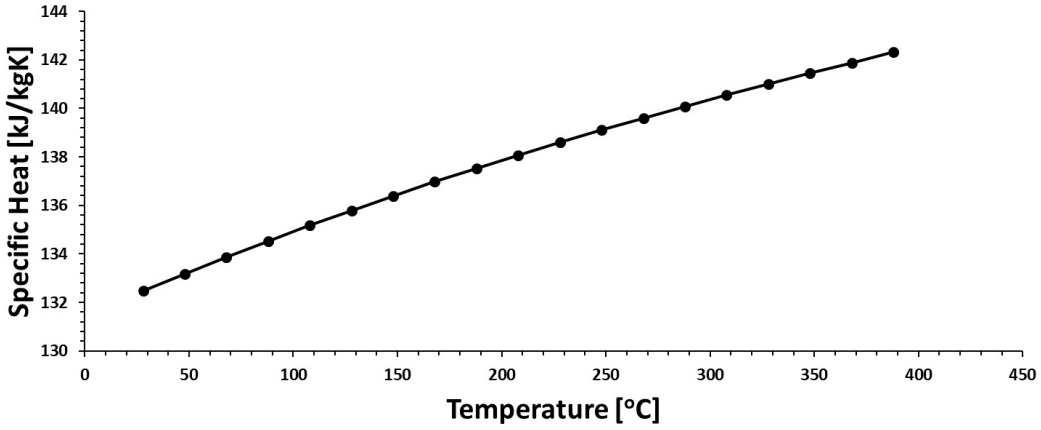

Figure A.4: ***Variation of specific heat of Tungsten with temperature***

B

User defined function for importing energy map

This section shows the UDFs used in the Fluent simulations for importing energy maps in the steady and the transient cases.

B.1. UDF for importing energy map in steady state case

```
#include "udf.h"
#include "stdio.h"
#include "math.h"
DEFINE_SOURCE(mypower_uds0,ce,t,dS,eqn)
{
#if !RP_HOST
double xvec[ND_ND];
C_CENTROID(xvec,ce,t);
/*Calculation of source term*/
        double source;
        source = 0.0;
        source = C_UDSI(ce,t,0);          /*uds-0*/
dS[eqn] = 0.0;
/*source = source / 7.2;*/
C_UDMI(ce,t,0) = source;
return source;
#endif
}
```

B.2. UDF for importing energy map in transient case

```
#include "udf.h"
#include "stdio.h"
#include "math.h"

DEFINE_SOURCE(mypower_uds0,ce,t,dS,eqn)
{
#if !RP_HOST
double xvec[ND_ND],t_current,t_pulse,t_cycle,t_norm;
C_CENTROID(xvec,ce,t);
t_current = CURRENT_TIME;
t_pulse = 1.0;
t_cycle = 7.2;
```

```
t_norm = t_current - t_cycle * floor(t_current / t_cycle);
/*Calculation of source term*/
        double source;
        if (t_norm < t_pulse) {
                source = C_UDSI(ce,t,0)*t_cycle;
                }
        else {
                source = 0.0;
        }
dS[eqn] = 0.0;
C_UDMI(ce,t,0) = source;
return source;
#endif
}
```

C

Mesh sensitivity analysis

It's quite challenging to perform mesh sensitivity analysis on the 3D model of the cooling system because of it's complex geometry, however and attempt was made to compare the results of two meshes. As illustrated in section 4.2.1, a mesh with around 19 million elements was used to perform the steady and transient analysis. In this appendix it's shown that even with a less dense mesh (having around 10 million elements), the results doesn't very too much as shown in figure C.1 and C.2 respectively.

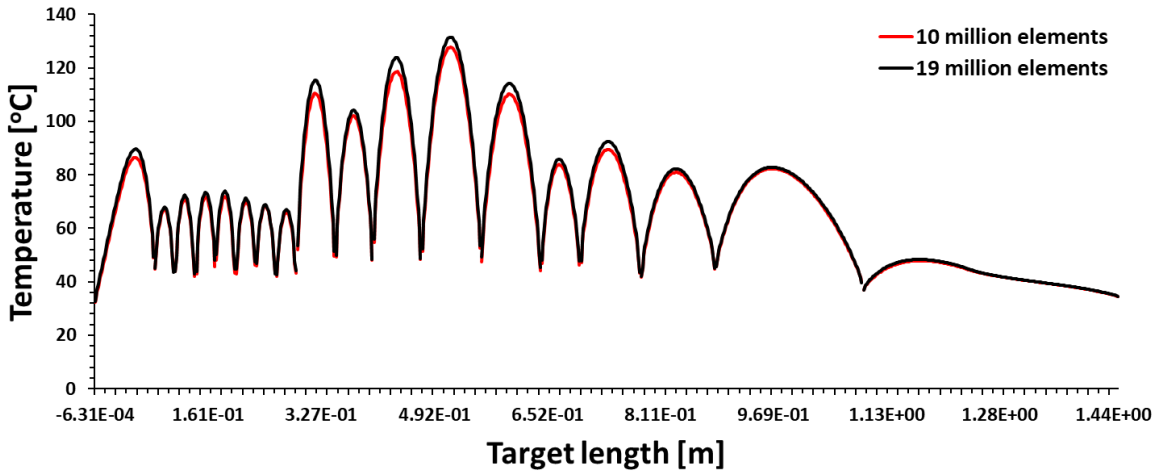

Figure C.1: ***Comparison between temperature profile in all blocks in steady state at 50mm from the axis of the target for two meshes having 10 million an 19 million elements respectively***

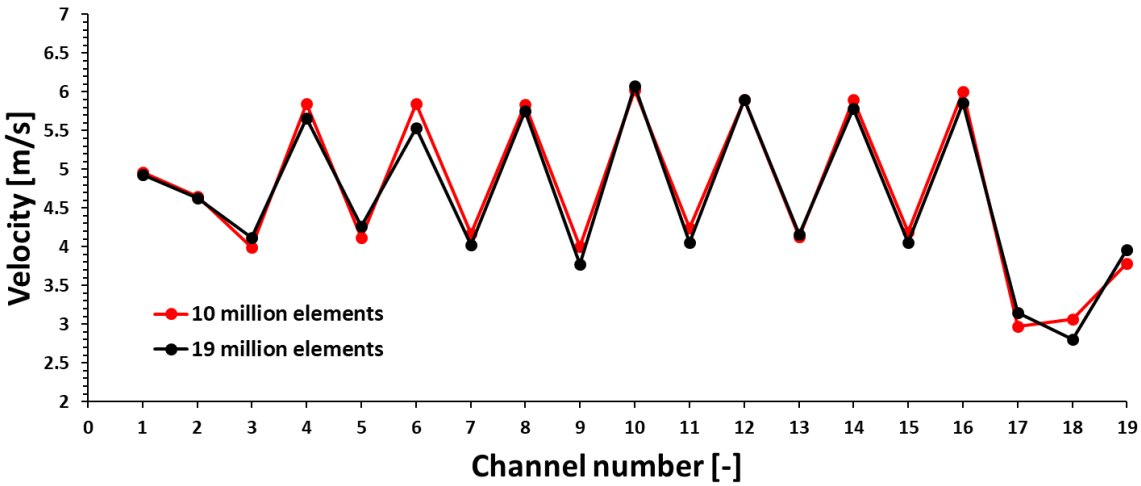

Figure C.2: ***Comparison between average velocity profile in all the channels for two meshes having 10 million an 19 million elements respectively***

Figure C.1 shows that a good comparison has been obtained between the temperature profiles in the target blocks at a distance of $50mm$ from the axis of the target for two different meshes. The maximum error here is less than 3%. Similarly, a good match can be seen in figure C.2 which illustrates the comparison between the average velocity in the channels for two different meshes. It can be concluded that around 50% reduction in the mesh density gives an error as large as 5-6%, however for the present cooling system very accurate results were desired and hence the mesh with 19 million elements was used for all the simulations.

D

Time step sensitivity analysis

A comparative analysis of the response of the transient case on the time step size is done in this appendix. Temperature profile in all the blocks at a distance of $50mm$ from the axis and the maximum temperature profile in block 12 is investigated against two different time step size, viz. 0.05 sec and 0.02 sec as shown in figures D.1 and D.2.

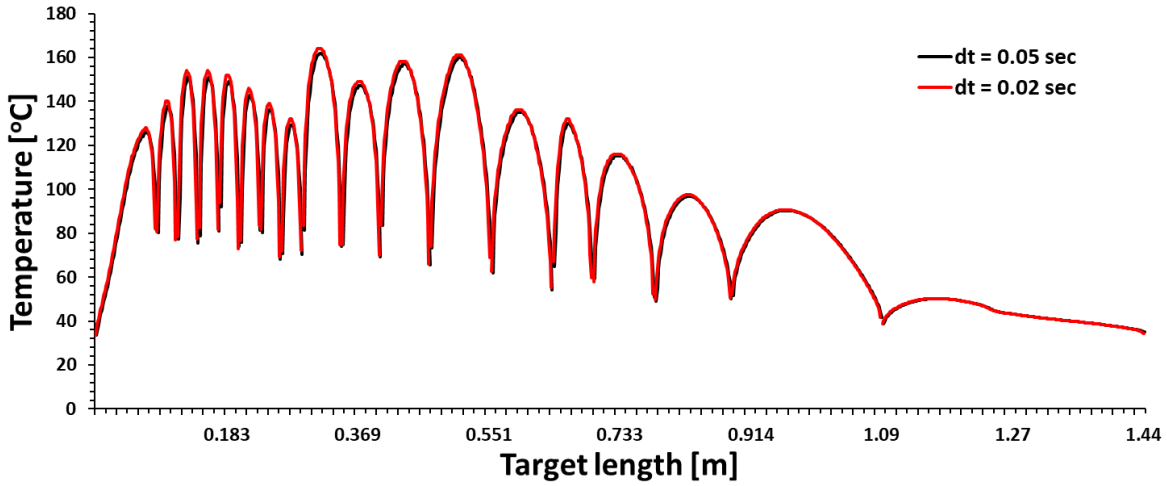

Figure D.1: ***Comparison between temperature profile in all blocks at the peak of the pulse for two different time step size: dt = 0.05 sec and dt = 0.02 sec***

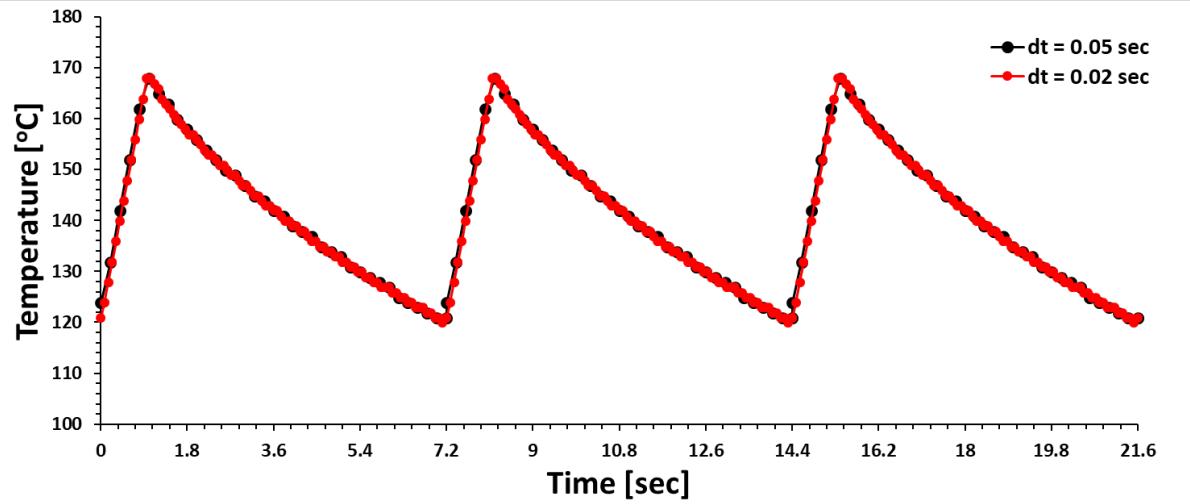

Figure D.2: ***Comparison between temperature profile in block 12 with time for two time step size: dt = 0.05 sec and dt = 0.02 sec***

As can be seen from the above figures, a good match has been obtained between two time step sizes and hence the choice of performing transient simulations at dt=0.05sec in section 4.2.3 is substantiated.

Bibliography

[1] Ansys Fluent 17.2. User guide. manual, 2016.

[2] Ansys Fluent 17.2. Theory guide. manual, 2016.

[3] A. J. Chorin. Numerical Solution of the Navier-Stokes Equations. *Mathematics of Computation, AMS*, 22:745–762, 1968.

[4] Adam Kraus, Elia Merzari, Tanju Sofu, Zhaopeng Zhong, and Yousry Gohar. CFD Analysis and Design of Detailed Target Configurations for an Accelerator-Driven Subcritical System. *Nuclear Technology*, 195:157–168, 2015.

[5] B. J. McKeon, M. V. Zagarola and A. J. Smits. A new friction factor relationship for fully developed pipe flow. *J. Fluid Mech*, 538, 2005. doi: 10.1017/S0022112005005501.

[6] B. S. Petukhov. Heat Transfer and Friction in Turbulent Pipe Flow with Variable Physical Properties. *Advances in Heat Transfer*, 6:503–564, 1970.

[7] Timothy Barth and Dennis Jespersen. The design and application of upwind schemes on unstructured meshes. In *27th Aerospace Sciences Meeting Reno,NV,U.S.A.* Technical Report AIAA-89-0366, 1989.

[8] Chaitanya M. Karale, Sunil S. Bhagwat and Vivek V. Ranade. Flow and Heat Transfer in Serpentine Channels. *AIChE, Wiley Online Library*, 59:1814–1827, 2013.

[9] Michel Chanel. Leir: The low energy ion ring at cern. In *8th European Particle Accelerator Conf., Paris, France*. EPAC, June 2002.

[10] Coles D. Measurements in the boundary layer on a smooth flat plate in supersonic flow; Part I. the problem of the turbulent boundary layer. *JPL/ CalTech. report no. 20-69*, 1953.

[11] Dan Wilcox, Peter Loveridge, Tristan Davenne, Leslie Jones and David Jenkins. Stress levels and failure modes of tantalum-clad tungsten targets at ISIS. *Journal of Nuclear Materials*, 15, 2017. doi: https://doi.org/10.1016/j.jnucmat.2017.10.075.

[12] P. Avigni E. Lopez Sola and J. Busom. Thermo-Mechanical and Cooling Design of the BDF Target Prototype Test and Comparison with the BDF Final Target. Technical report, European Organization for Nuclear Research (CERN), 01 2018.

[13] M. Lamont et al. The sps beam dump facility. In *8th Int. Particle Accelerator Conf., Copenhagen, Denmark*, pages 2389–2391. IPAC 2017, May 2017.

[14] Quan Ji et al. Physics Design and Technology Development of CSNS Target Station and Instruments. Technical report, Institute of High Energy Physics, Institute of Physics, CAS, 04 2010.

[15] M. A. Clark-Gather G. M. Allen, T. A. Broome and C. W. Planner. Measurement of cooling characteristics of the isis tantalum target. In *Proceedings of ICANS XII, pT12*, volume 2. RAL 94-025, May 1993.

[16] G.W. Maurer and B.W. LeTourneau. Friction Factors for Fully Developed Turbulent Flow in Ducts With and Without Heat Transfer. *Journal of basic engineering*, sep 1964.

[17] J. Dirker and J. P. Meyer. CONVECTION HEAT TRANSFER IN CONCENTRIC ANNULI. *Experimental Heat Transfer*, 17:19–29, 2004. doi: 10.1080/08916150490246528.

[18] J.J Allen, M.A Shockling, G.J Kunkel and A.J Smits. Turbulent flow in smooth and rough pipes. *Philos Trans A Math Phys Eng Sci.*, 15, mar 2007.

[19] J.P Hartnett, J.C.Y. Koh and S.T. McComas. A Comparison of Predicted and Measured Friction Factors for Turbulent Flow Through Rectangular Ducts. *Transactions of the ASME*, feb 1962.

[20] Junjia Cui, Chengxi Le, Zhongwen Xing, Chunfeng Li and Shumei Ma. Predictions of the Mechanical Properties and Microstructure Evolution of High Strength Steel in Hot Stamping. *Journal of Materials Engineering and Performance, Springer*, 21, 11 2012. doi: https://doi.org/10.1007/s11665-012-0180-9.

[21] K.J. Harder and W.G. Tiederman. Drag reduction and turbulent structure in two-dimensional channel flows. *Philos Trans R. Soc. Lond. A*, 336:19–34, 1991.

[22] R. Betemps J.-L. Grenard-D. Horvath P. Pacholek A. Perez A. Perillo Marcone A. Rakai R. Rinaldesi S. Sgobba C. Strabel V. Venturi M. Calviani, M. Battistin and H. Vincke. Conceptual design of the SHiP Target and Target Complex. Technical report, European Organization for Nuclear Research (CERN), 05 2015.

[23] M. Nallasamy. TURBULENCE MODELS A N D THEIR APPLICATIONS TO THE PREDICTION OF INTERNAL FLOWS: A REVIEW. *Computers and Fluids*, 15:151–194, 1987.

[24] Menter, F. R. Zonal Two Equation k-ω Turbulence Models for Aerodynamic Flows. *AIAA-93-2906*, 2 1993. doi: 10.2514/6.1993-2906.

[25] Muhammad Ahsan. Numerical analysis of friction factor for a fully developed turbulent flow using $k-\epsilon$ turbulence model with enhanced wall treatment. *Beni-Suef Journal of Basic and App. Sc. (Elsevier)*, pages 269–277, 2014.

[26] A. Benzaoui N. El Gharbi, R. Absi and E.H. Amara. Effect of near wall treatments on airflow simulations. In *Int. Conf. on Computational Methods for Energy Eng. and Env.*, pages 185–189. ICCM3E 2009, November 2009.

[27] Paride Meloni and Massimiliano Polidori. A neutronics–thermalhydraulics model for preliminary studies on TRADE dynamics. *Nuclear Engineering and Design*, 237:1704–1717, 2007.

[28] Patankar S. V. and Spalding D. B. A Calculation Procedure for Heat, Mass and Momentum Transfer in Three-Dimensional Parabolic Flows. *Int. J. Heat Mass Trans.*, 15: 1787–1806, 1972.

[29] Aniko Rakai and Piotr Pacholek. SHiP target area CFD studies. Technical report, European Organization for Nuclear Research (CERN), 01 2015.

[30] R.B. Dean. Reynolds number dependence of skin friction and other bulk flow variables in two-dimensional rectangular duct flow. *Journal of Fluids Engineering*, 100, jun 1978.

[31] R.H.S.Winterton. Where did the Dittus and Boelter equation come from? *Int. Journal of Heat and Mass Transfer*, 41, March 1998. doi: https://doi.org/10.1016/S0017-9310(97)00177-4.

[32] Robert D. Moser, John Kim and Nagi N. Mansour. Direct numerical simulation of turbulent channel flow up to Re_τ =5590. *Physics of Fluid*, 11, apr 1999.

[33] S. Maharudrayya, S. Jayanti and A.P. Deshpande. Pressure losses in laminar flow through serpentine channels in fuel cell stacks. *Journal of Power Sources*, 138:1–13, 2004.

[34] Sergey Alekhin et al. A facility to search for hidden particles at the CERN SPS: the SHiP physics case. *Rep. Prog. Phys.*, 79, 10 2016. doi: 10.1088/0034-4885/79/12/124201.

[35] JAHM software. Material properties database. software, 2018.

[36] Raffaello Sobbia Sven Jollet and Michael Wohlmuther. Numerical flow simulation of the neutron source sinq of psi. In *Journal of Physics: Conference Series*, volume 1021, 2018. doi: 10.1088/1742-6596/1021/1/012063.

[37] F. P. Incropera T. L. Bergman, A. S. Lavine and D. P Dewitt. *Fundamentals of Heat and Mass Transfer*, chapter 8. Internal Flow. John Wiley and Sons, 2011.

[38] T. Wei and W. w. Willmarth. Reynolds-number effects on the structure of a turbulent channel flow. *J. Fluid Mech*, 204, 1989.

[39] T.T. Bohlen et al. The FLUKA Code: Developments and Challenges for High Energy and Medical Applications. *Nuclear Data Sheets*, 120:211 – 214, 2014. ISSN 0090-3752. doi: {https://doi.org/10.1016/j.nds.2014.07.049}. URL http://www.sciencedirect.com/science/article/pii/S0090375214005018.

[40] V. Gnielinski. New Equations for Heat and Mass Transfer in Turbulent Pipe and Channel Flow. *International Chemical Engineering*, 16:359–368, 1976.

[41] Dan Wilcox. Design and optimisation of the isis ts1 upgrade target. In *6th High Power Targetry Workshop*, 2016.

[42] X. Cheng, P.J. Finck, J. Roglans-Ribas and T. Schulenberg. Thermal-hydraulic design analysis of a 5 MW sodium-cooled tungsten target. *International Nuclear Information System*, 49, 2003.

[43] Xu Cheng, Abdalla Batta, Nan-I1 Tak, Ferry Roelofs and Pablo T. Leon Lopez. Thermal-hydraulic analysis of the TRADE spallation target. *Nuclear Instruments and Methods in Physics Research A*, 562:855–858, 2006.